https://ntrs.nasa.gov/search.jsp?R=19960012495 2020-06-16T04:43:27+00:00Z

NASA Contractor Report 198267

NASA-CR-198267
19960012495

Simulation of Crossflow Instability on a Supersonic Highly Swept Wing

C. David Pruett
The College of William and Mary, Williamsburg, Virginia

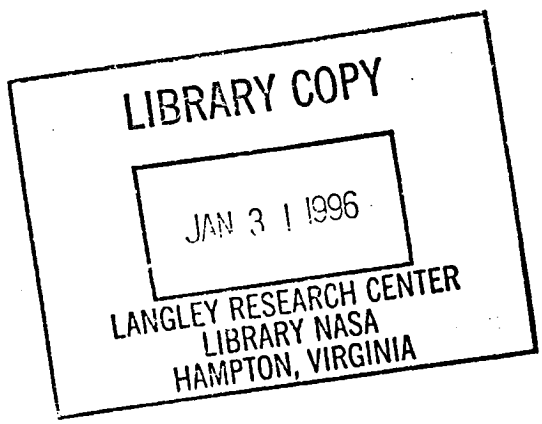

Contract NAS1-19656

October 1995

National Aeronautics and
Space Administration
Langley Research Center
Hampton, Virginia 23681-0001

NASA Technical Library
3 1176 01423 8258

SIMULATION OF CROSSFLOW INSTABILITY ON A SUPERSONIC HIGHLY SWEPT WING

Dr. C. David Pruett
Department of Applied Science
The College of William and Mary

Abstract

A suite of highly accurate numerical algorithms has been developed and validated for use in the simulation of crossflow instabilities on supersonic swept wings, an application of potential relevance to the design of the High-Speed Civil Transport (HSCT). Principal among these algorithms, and the primary focus of this report, is a direct numerical simulation (DNS) scheme embodied in the code CMPSBL, which solves the unsteady, three-dimensional compressible Navier-Stokes equations in orthogonal, body-fitted coordinates. The DNS algorithm is fully explicit in time and exploits a combination of spectral and high-order compact-difference techniques for spatial discretizations. A companion code WINGBL2, documented in a previous technical report, exploits spectral-collocation techniques to solve the compressible boundary-layer equations to provide an accurate basic state to the DNS. In addition, the algorithm INTBL uses spectral techniques to interpolate the boundary-layer solution onto the computational grid of the DNS. These algorithms are then used to examine the development of stationary crossflow instability on an infinitely long 77-degree swept wing in Mach 3.5 flow. Crossflow disturbances are generated by simulating spanwise-periodic roughness elements downstream of the computational inflow boundary. The results of the DNS are compared with the predictions of linear parabolized stability equation (PSE) methodology obtained with the code ECLIPSE (developed independently of this effort). In general, the DNS and PSE results agree closely, thereby providing a reasonable validation of both approaches. Specifically, both methods show the alignment of stationary crossflow vortices along inviscid streamlines as anticipated. Moreover, the methods agree well in the predicted spatial evolution of a small-amplitude (linear) crossflow mode and in the structure of this mode. Although further validation is warranted (for large-amplitude stationary and traveling crossflow disturbances), the present results demonstrate a new numerical capability relevant to a problem of practical importance.

1 Introduction

Understanding, predicting, and controlling laminar-turbulent transition remains the holy grail of aeronautics research despite more than a century of assault from the combined forces of theory, experiment, and computation. Recent advances on each of these fronts and in the areas of materials processing and micro-actuators (Ho and Tai [13]), however, have brought this elusive goal within sight, and there is renewed interest in laminar-flow control (LFC) technology.

Because surface friction and heat transfer increase dramatically as the boundary layer transitions from a laminar to a turbulent state, the design of efficient aerospace vehicles depends upon accurately predicting the transition location and the extents of the regions of laminar, transitional, and turbulent flows. Although, in the current economic environment, it is questionable whether laminar flow control (LFC) technology can be made commercially viable in the near future for subsonic aircraft, the potential economic benefit could be significant for supersonic transport aircraft such as the proposed High-Speed Civil Transport (HSCT). This is because maintenance of laminar flow over a substantial portion of the wing of the HSCT, for example, would not only reduce drag but would also reduce thermal loads on the structure.

The practical attainment of LFC technology will require fundamental understanding of the stability of three-dimensional boundary-layer flows. Examples of prototypical three-dimensional boundary-layer flows are flows past rotating cones and spheres, flow on a rotating disk, flows in corners, and flows over swept wings, the latter of which is of the most practical relevance.

Whereas the stability of two-dimensional flows has been studied extensively, researchers are only beginning to focus attention on three-dimensional boundary-layer flows. Theoretical and experimental results demonstrate that there exists a far greater variety of paths to transition for three-dimensional boundary layers than for two-dimensional flows. For example, in the case of the swept wing, the flow may be susceptible to Tollmien-Schlicting (TS) instability, Goertler instability (associated with the concavity of the lower surface; e.g., see Hall [12]), crossflow instability (the subject of the discussion to follow), and attachment-line instability (instability of the flow along the leading edge; e.g., see Joslin [17]). For the wing of the HSCT, to be specific, crossflow instability is likely to be the most "dangerous" in the sense of leading most rapidly to transition.

Crossflow instability was first identified in the 1940's in experiments related to the Northrop flying wing. As stated by Reed and Saric [28] in their review paper, "Although unyawed wind-tunnel tests showed laminar flow back to 60 percent chord, yawed flight tests showed turbulent flow from the leading edge on both the upper and lower surfaces." In flow over a swept wing, the inviscid streamlines form S-curves because the pressure gradients associated with body curvature accelerate or decelerate the flow in the direction perpendicular to the leading edge while leaving the velocity component parallel to the leading edge

virtually unchanged. The combination of curvilinear inviscid streamlines and the viscous no-slip condition at the wall generates a crossflow velocity perpendicular to the local inviscid streamline. The crossflow velocity is zero both at the wall and in the freestream (by definition), and thus, in between it experiences a maximum and a point of inflection. Maxima for crossflow velocities are typically on the order of 3-4 percent of the velocity in the direction of the streamlines.

Even though crossflow velocities are typically relatively small, the presence of the inflection point renders the flow susceptible to crossflow instability, which is of inviscid type. The instability manifests itself as co-rotating vortices that align themselves roughly along inviscid streamlines. The spacing between adjacent vortices is on the order of several δ^*, the boundary-layer displacement thickness. According to Mack [20], the instability exists for a whole band of frequencies, including zero. Curiously, linear stability theory predicts the most amplified disturbances to be traveling waves, whereas stationary crossflow instability is frequently observed in experiments, except close to laminar breakdown (Reed and Saric [28]). Choudhari and Streett [10] and Choudhari [9] have shown, on the basis of receptivity theory, that surface irregularities may favor the development of stationary crossflow modes by giving them much larger initial amplitudes than those of traveling crossflow waves.

Both theory and experiment concur that crossflow instability dominates on swept wings in regions of rapidly changing pressure. Other regions on the wing, however, may be dominated by TS-like instabilities (which we take to include the first-mode instability of compressible boundary-layer flow). According to Reed and Saric [28], a major unanswered question is "the interaction between crossflow vortices and TS waves." It appears that crossflow vortices can modify the TS instability to enhance its growth rate. From experiments, it also appears that the crossflow instability is extremely sensitive to initial conditions, and it has even been suggested that the theory for crossflow instability is not well posed (Reed and Saric [28]).

In summary, transition on a swept wing is a highly sensitive and complex process. The transition location is affected by nonparallelism of the mean flow, pressure gradient, surface roughness, freestream turbulence, and body curvature. Moreover, these elements give rise to both inviscid crossflow modes and to TS-like instabilities, which may interact. It is unreasonable to ask any approximate theory to accommodate all of these diverse and interacting elements. As a result, the problem is well suited for numerical investigations using direct numerical simulation (DNS), for which a minimum of simplifying assumptions are made.

Crossflow instability on swept wings in incompressible flows has been investigated recently with a parabolized stability equation (PSE) approach by Malik et al. [21] and with DNS by Lin and Reed [19], Fuciarelli and Reed [11], Joslin and Streett [18], and Joslin [16]. The present work is believed to be the first investigation of crossflow instability on a supersonic swept wing by means of DNS. Direct simulation is computationally expensive; consequently, we believe that simulations are most fruitful when focused along with theoretical and experimental investigations on a single problem of practical importance. To that end, we have selected a test problem that parallels the quiet wind-tunnel experiment on a supersonic swept wing by Cattafesta et al. [3]. Moreover, our DNS results are compared

with results obtained by PSE methodology for compressible flows (e.g., Chang et al. [6]) in an attempt to cross-validate both methods for this difficult problem. For computational efficiency, we must limit consideration to quasi-three-dimensional (infinite-span) swept-wing flows. This assumption permits highly efficient spectral collocation methods to be exploited in the spanwise direction. The limitation of the computational model should be kept in mind in drawing conclusions relative to the experiment. We emphasize, however, that the full effects of streamwise surface curvature are incorporated into the DNS model, in contrast to most recent approaches.

The next section discusses the coordinate system and governing equations. Section 3 summarizes the numerical methodology. The computational test case is addressed in Section 4. Results are presented in Section 5, and Section 6 concludes with a few closing remarks.

2 Governing Equations

The flow is governed by the compressible Navier-Stokes equations in the form given in Eqs. (1)-(15) of Pruett et al. [26], which is appropriate for body-fitted coordinates on either axisymmetric or two-dimensional bodies. Here, we consider only two-dimensional (infinite in span) wing-like bodies. Let the wing be imbedded in a rectangular cartesian coordinate system (ξ, η, ζ), with the wing cross section specified as $\zeta(\xi)$. Let (x, y, z) denote body-fitted coordinates such that x is the surface arc length normal to the attachment line, y is the spanwise coordinate (parallel to the attachment line), and z is the wall-normal coordinate. (The reader will note that, for consistency with the coordinates of Pruett et al. [26], the y and z coordinates are switched relative to the normal convention.) Accordingly, u, v, and w are the velocity components in the streamwise, spanwise, and wall-normal directions, respectively. The fundamental metric tensor has only one non-constant quantity s, which arises from streamwise curvature and is defined in Eq. (2) of Pruett et al. [26]. Moreover, by ρ, p, T, μ, and κ, we denote the density, pressure, temperature, viscosity, and thermal conductivity of the fluid, respectively. The viscosity μ is modeled by Sutherland's law, and $\kappa = \mu/Pr$, where Pr is the Prandtl number. For computational efficiency, the energy equation is cast in terms of the pressure, as given in Eq. (15) of Pruett et al. [26]. All flow variables, except pressure, are non-dimensionalized by post-shock reference values, denoted by subscript r. Pressure is scaled by $\rho_r^* u_r^{*2}$. Lengths are scaled by the boundary-layer displacement thickness δ^* at the (computational) inflow boundary. Throughout this work, dimensional quantities are denoted by asterisk.

3 Methodology

The conventional approach to (spatial) stability analysis, adopted here, consists of three basic steps: determination of a laminar base state whose stability is to be investigated,

perturbation of the base state by superposition of disturbances at or near the computational inflow boundary, and calculation of the spatial evolution of the disturbances. Each of these steps is addressed in turn below.

3.1 Base Flow

The base state is computed by the spectrally accurate boundary-layer code WINGBL2 of Pruett [25], which was specifically designed for the infinite-span swept-wing problem. The effects of streamwise curvature, streamwise pressure gradient, and wall suction/blowing are taken into account in the governing equations and boundary conditions. The boundary-layer equations are formulated both for the attachment-line flow and for the evolving boundary layer. The equations for the evolving flow are solved by an implicit marching procedure in the direction perpendicular to the leading edge, for which high-order (up to 5th) backward differencing techniques are used. In the wall-normal direction, a spectral collocation method based on Chebyshev polynomial approximations is exploited. Spectral accuracy is advantageous in that 1) the solution is highly accurate even for relatively coarse grids, 2) the boundary-layer profiles and their derivatives are extremely smooth (a necessity for stability analyses), and 3) interpolation to other grids can be accomplished with virtually no loss of accuracy.

A few comments in regard to point 3) above are in order. Because WINGBL2 is designed specifically for applications to stability analyses, DNS, and large-eddy simulation (LES), special attention has been paid to the process of interpolating data to other grids, for example, to a DNS grid. For this purpose, a companion code INTBL was written. In brief the procedure is as follows. In the output from WINGBL2, lengths are scaled by δ^*, which grows with x^*. The outer edge of the boundary layer typically lies between 2 and 4 displacement thicknesses from the wall. Let $z_e(x)$ denote the location of the boundary-layer edge. To interpolate to a grid uniform in z, for example, we first perform spectrally accurate interpolation in the interior region $0 \leq z \leq z_e$ coupled with analytic extrapolation outside the boundary layer ($z > z_e$). This step is followed by high-order (typically 5th) polynomial interpolation in x.

The analytic extrapolation in the far field is accomplished at each x by solving the ordinary differential equation that results from the continuity equation in the asymptotic limit $z \rightarrow \infty$. In many boundary-layer approximations, some curvature effects are neglected, in which case the continuity equation may be inexact. Indeed, it was determined that Eq. (7-100) on page 397 of Anderson et al. [1], on which the continuity equation for WINGBL2 was originally based, is inexact for compressible flow; an exact continuity equation was subsequently derived. That the continuity equation be exact is essential if the near-field solution and the far-field extrapolation are to merge continuously, as they must for DNS. The method proposed by Pruett [24] to extract wall-normal velocity accurately, adopted here also, permits an independent check of continuity. Typically WINGBL2 conserves continuity nearly to machine precision, as shown in Figs. 1 and 2.

The input to WINGBL2 consists primarily of three files that contain the wing geometry, the wing pressure distribution in the form of tabulated pressure coefficients, and the reference conditions. Cubic splines are used to interpolate as necessary between the tabulated values. The reference conditions are presumed to be downstream of leading-edge shocks.

3.2 Disturbances

The base flow is perturbed in the manner of Joslin [16], who simulated crossflow instability in incompressible flow on a swept wing. Disturbances are introduced by mass-preserving suction and blowing at the wall. Currently, we exploit steady suction/blowing in order to induce stationary crossflow modes. The suction/blowing strip spans the width of the wing, but is localized in x. (Henceforth, for brevity, we will refer only to the "suction" strip.) As noted by Joslin [16]: "This mode of disturbance generation would correspond to an isolated roughness element within the computational domain." Joslin has found by numerical experimentation that the suction strip should not be located farther upstream than approximately 10 percent chord. Otherwise, the crossflow modes are not swept downstream. The spanwise wavenumber β of the disturbance strip is a fundamental parameter of the flow, as is the maximum amplitude of the wall velocity w_{wall}. Typically, very small normalized wall velocities (say, $w_{\text{wall}} = 10^{-4}$ or less) suffice to trigger stationary crossflow instability. The suction/blowing profile is a full sine wave in the spanwise direction; to ensure continuity of derivatives, the cube of a half sine function is used to shape the wall velocity in the streamwise direction.

3.3 DNS Methodology

For the present application, we exploit the highly accurate DNS methodology of Pruett et al. [26] with minor modifications. To summarize briefly, time is advanced fully explicitly by the third-order low-storage Runge-Kutta scheme of Williamson [30]. Spatial derivatives are approximated by a combination of spectral-collocation techniques and high-order compact-difference schemes. In the streamwise and wall-normal directions, we exploit fourth- and sixth-order compact-difference operators, respectively. In the spanwise direction, the flow is assumed to be periodic, making possible the use of a spectral collocation technique with Fourier exponential basis functions. The assumption of spanwise periodicity restricts the basic flows under consideration to quasi-three-dimensional; that is, all base-flow quantities, including the three velocity components, are assumed to be functions only of the streamwise and wall-normal coordinates. This is equivalent to assuming that the wing is of infinite span with constant cross-section.

The boundary conditions require some modification from those given in Pruett et al. [26]. For a well-designed wing, the streamwise component of velocity should be everywhere subsonic. Therefore, the streamwise velocity at the computational inflow boundary is subsonic,

and in the outer (Euler) region of the domain, there exists an upstream characteristic velocity. Accordingly, we specify the Riemann invariants along the inflow boundary. This inflow treatment, correct for inviscid flow, is not entirely satisfactory in the viscous layer, where all flow quantities should be specified (Poinsot and Lele [22]). The wall and far-field boundary treatments are the same as described in Pruett et al. [26], except that suction and blowing are introduced at the wall to induce the disturbance, as described previously. We currently exploit a buffer domain (Streett and Macaraeg [29]) in the vicinity of the outflow boundary, as was done successfully by Pruett et al. [26]. However, for this particular application, we are presently experiencing some reflection from the outflow boundary. It is not yet known whether the reflection is of numerical or physical origin (or both). Additional effort should be directed to diagnosis and refinement of the inflow and outflow boundary conditions.

The work of Pruett et al. [26] and the present work differ conceptually in that, for the latter, which is concerned with stationary crossflow instability, only the time-asymptotic solution is of interest. Time integration is accomplished solely as a means of relaxation toward the steady state. Physically, from the point at which a disturbance is introduced, a wave packet propagates (predominantly) downstream, depositing in its wake the stationary crossflow instability of interest. Once the leading wave packet has exited the domain, the flow settles to its perturbed steady state. Attainment of a steady state is assessed by computing the residuals of the time-independent compressible Navier-Stokes equations. In practice, in the context of fully explicit time advancement, the residual is simply the discrete update vector. Evolution of the global maximum residual for the calculation of the "Results" section is shown in Fig. 3. The largest residuals are associated with the continuity (ρ) and spanwise momentum (v) equations. The maximum residuals grow approximately exponentially in time as the leading wavefront propagates downstream at a nearly constant velocity, as implied by Fig. 4. Different formulations for the buffer domain may change the velocity of propagation in this region. For example, the buffer domain treatment that resulted in the least reflection also unfortunately significantly diminished the propagation velocity in the buffer region, necessitating a relatively long integration time. Following the exit of the leading wavefront from the domain (not shown), the residuals decay rapidly, provided the outflow boundary treatment is non-reflecting. Moreover, examination of the local residual field (also not shown) indicates that the flow is essentially stationary a short distance upstream of the trailing edge of the propagating wave packet. Finally, Fig. 5 shows the location of the maximum residual in terms of the wall-normal gridpoint index k. The initial outward movement of the residual is associated with a weak acoustic pulse that radiates from the receptivity region near the suction strip. Following the exit of this wave from the upper boundary, the maximum residual remains near $k = 40$, a distance of approximately $1.5\delta^*$ from the wall, until the wave encounters the buffer domain. The wall-normal location of maximum residual coincides closely with the maximum perturbation amplitude of the crossflow instability.

3.4 PSE Methodology

The PSE method, developed originally for incompressible flow, has been extended to compressible boundary layers by Bertolotti and Herbert [2] and by Chang and coworkers (See references [4] and [7]). The method is rapidly gaining favor as a powerful and efficient tool for analyzing the stability of spatially evolving boundary layers. The method treats both nonparallel boundary-layer effects and moderately nonlinear wave interactions. The method has recently been adapted for application to supersonic swept wings by Chang and coworkers. The theory is presented in Reference [6]; a user-friendly code ECLIPSE for industry applications has also been developed and is documented in Reference [5]. The reader is referred to these references for a thorough discussion of the theory and practice of PSE methodology.

4 Test Problem

As implied in the introduction, the computational experiment is an approximate analog to the quiet wind-tunnel experiment of Cattafesta et al. [3]. In this section, we compare and contrast the physical and numerical experiments.

4.1 The physical experiment

The reader is referred to Cattafesta et al. [3], which is summarized briefly here. A 15-inch-long model of a wing section with a leading-edge sweep angle $\psi = 77.1^{\circ}$ is being tested in NASA Langley's Mach 3.5 quiet wind-tunnel to investigate crossflow instability and transition. A three-dimensional view of the model is shown in Fig. 2 of Cattafesta et al. [3]. The model was designed originally to experience flow similar to that on the 70-degree swept wing of an F-16XL, which is undergoing flight experiments by NASA. The model cross section is geometrically similar to that of the first 6.25 percent chord of the wing glove on the modified F-16XL. However, the sweep angle on the wind-tunnel model was increased to 77 degrees to match the leading-edge-normal Mach number of the Mach 3.5 wind-tunnel experiment to that of the Mach 2.4 flight experiment, for which the normal Mach number is 0.78.

Because crossflow-dominated transition is quite sensitive to controlled and random influences, it was deemed necessary to conduct the experiment in a quiet facility. In the physical experiment, the freestream unit Reynolds numbers were varied from 1.5 to 8.0 million per foot by varying the tunnel stagnation pressure, and the angle of attack was incremented from -2 to 5 degrees. In support of the experiment, Euler and Navier-Stokes calculations were conducted, as were N-factor studies using the stability code COSAL (Iyer et al. [15]). As in most theoretical studies of crossflow instability, traveling waves were predicted to have the highest growth rates; peak N-factors were observed for frequencies in the range of 40

to 60kHz. The transition front on the model was estimated on the basis of recovery factors obtained from surface thermocouples. More recently, temperature-sensitive paint has been used to more finely resolve the transition front. The measured and predicted transition fronts correlated approximately for $N = 14$. However, regions on the model with microscopic surface scratches showed the telltale streaks of stationary crossflow vortices.

4.2 The numerical experiment

Data for the numerical experiment were inferred from an Euler calculation of the flow on the wing model by Iyer [14], for which the freestream conditions were

$$M_\infty = 3.5 \quad (1)$$
$$T_\infty = 173.9^\circ \text{ R} \quad (2)$$
$$Re_1 = 2.6 \times 10^6 \text{ per ft.} \quad (3)$$
$$\alpha = 0.145^\circ \quad (4)$$

Fig. 6 shows isobars on the upper and lower surfaces of the model for the freestream conditions given above. Near the aft stations on the wing, the wing sections are similar (Cattafesta et al. [3]), and the isobars are nearly parallel, which suggests that the flow can be approximated as quasi-three-dimensional (although Cattafesta et al. caution against this). Accordingly, we consider a wing section perpendicular to the leading edge at a station 1.091 ft. along the leading edge, as shown in Fig. 7. The chord length c_n^* normal to the leading edge at the section of interest is 0.2496 ft. The surface pressure coefficients interpolated from the Euler grid to the wing section are shown in Fig. 8. The surface pressure coefficients were then used as input data for the boundary-layer code WINGBL2 (described earlier) to derive the base state. Some additional interpretation of the Euler data, however, was necessary to provide post-shock reference conditions to the boundary-layer code. From the Euler data, the post-shock Mach number at the point of maximum wingspan was taken to be 3.29. Because of the outward turning of the flow through the shock, the effective wing sweep angle ψ_{eff} increased by a few degrees over the physical value. Finally, the post-shock reference temperature was adjusted to force agreement between the Euler and boundary-layer stagnation temperatures. These self-consistent post-shock reference values are summarized as follows:

$$M_r = 3.29 \quad (5)$$
$$T_r = 189.6^\circ \text{ R} \quad (6)$$
$$u_r = 2220.4 \; f/s \quad (7)$$
$$p_r = 64.06 \text{ psia} \quad (8)$$

$$\psi_{\text{eff}} = 80.81^{\circ} \tag{9}$$

From the geometry, reference values, and pressure coefficients, the boundary-layer solution was computed based on the approximation of isentropic post-shock flow. The boundary-layer and Euler solutions for the edge Mach number and edge temperature are compared in Figs. 9 and 10, respectively. The small disagreement between the two solutions can be attributed to two sources. First, although the shock is weak, shock strength varies in azimuth due to the asymmetry of the body. Consequently, the post-shock flow is not strictly isentropic. Second, of course, the base flow is not perfectly two-dimensional. Nevertheless, the close agreement between the two solutions suggests that the simplifying assumptions are reasonable.

Growth of the boundary-layer displacement thickness, obtained from WINGBL2, is presented in Fig. 11. The favorable pressure gradient induces a boundary layer that grows linearly, except during the most rapid acceleration near the leading edge. The boundary-layer solution is compared at two stations, $x_c \equiv \xi^*/c_n^* = 0.0$ and $x_c = 0.173$, in Figs. 12 and 13, which show velocity and temperature profiles, respectively. By definition, of course, the streamwise velocity vanishes along the attachment line, which corresponds (nominally) to $x_c = 0.0$. Figure 14 shows the solution also at $x_c = 0.173$, but in a coordinate system oriented along the inviscid streamline. In the rotated coordinated system, u_t^* and u_c^* denote the tangential and crossflow velocities, respectively. Note the inflectional nature of the crossflow velocity (the component perpendicular to the inviscid streamline). The crossflow Reynolds number, defined in Reed and Saric [28], is shown as a function of x_c in Fig. 15. The maximum crossflow Reynolds number is attained at approximately 20 percent chord and decreases gradually thereafter.

Finally, the boundary-layer solution is interpolated onto the DNS grid by the interpolation code INTBL described previously. The computational domain for the DNS spans approximately from 1 to 70 percent chord in streamwise extent and from the wall to $z = z^*/\delta^* = 25$ in wall-normal extent. At the inflow boundary, $\delta^* = 0.00053$ ft. An algebraic mapping is used in the wall-normal direction to cluster points close to the wall. A second (linear) mapping is used to remove the major effects of the boundary-layer growth shown in Fig. 11, so that the boundary layer remains of nearly constant thickness in the scaled coordinate $z^*/\delta^*(x^*)$. N-factor studies by Chang [8], who used PSE methodology, determined that a stationary crossflow mode of spanwise wavelength $\lambda_y^* = 10$ mm (0.0328 ft.) was strongly amplified. Accordingly, the fundamental spanwise wavenumber was chosen to be $\beta \equiv \beta^*\delta^* = 2\pi\delta^*/\lambda_y^* = 0.1018$. The width of the computational domain was one spanwise wavelength; that is, $1 \times \lambda_y^* = 0.0328$ ft. The suction strip spanned from 6.7 to 9.6 percent chord, and $w_{\text{wall}} = 10^{-4}$.

5 Results

The DNS calculation was made with a resolution of $577 \times 4 \times 97$ in the streamwise, spanwise, and wall-normal directions, respectively. The streamwise and wall-normal resolutions were based on the DNS experience of Joslin [16] and of Pruett and Chang [27]. The spanwise resolution was sufficient to resolve only the mean and a single crossflow mode; hence, dealiasing was exploited (in Fourier space) in the spanwise direction to remove energy in the first harmonic of the spanwise fundamental.

To establish the crossflow disturbances throughout the domain required an integration in time to approximately $t = 1800$, at which time the leading wavefront had encountered the outflow boundary. Because the present outflow conditions are not completely satisfactory, a fraction of the incident energy was reflected by the boundary and contaminated the upstream solution. Hence, the computation was halted prior to the exit of the leading wavefront from the domain. Fig. 16 shows the evolution of the maximum of the (dealiased) perturbation spanwise velocity as a function of the streamwise coordinate. Superimposed on the plot is the amplitude of the v component of the crossflow instability as predicted by linear PSE methodology. The initial amplitude of the PSE result is arbitrarily scaled for the purpose of comparison. In the vicinity of the suction strip, where receptivity is enhanced, spatial transients are observed. Downstream of the suction strip, apparently a stationary crossflow mode is established, which grows in close agreement with the prediction of linear PSE. The leading wave packet is broad and spans approximately $0.35 \leq x_c \leq 0.7$ at termination of the calculation. Moreover, by comparison with the linear PSE result, it appears that the leading wave packet experiences amplitudes one to two orders of magnitude larger than the crossflow instability that is deposited by its passing. Thus, despite the initially low amplitude of the disturbance, strong nonlinearities are encountered as the leading wavefront passes. Indeed, in a previous simulation with a different buffer-domain treatment, in which the wavefront completely exited the computational domain, nonlinearities and their associated Lighthill stresses were strong enough in the wave-packet region to generate significant acoustic energy, as shown in Fig. 17. Following passage of the wavefront, the acoustic radiation vanished.

Figure 16 suggests that a linear crossflow mode has been established in the DNS calculation in the region $0.10 \leq x_c \leq 0.35$. Further confirmation of this is evidenced in Fig. 18, which compares the amplitude of the fundamental spanwise Fourier harmonic of the DNS calculation with the amplitude of the crossflow mode predicted by the PSE method at the station $x_c = 0.22$. For the comparison, the PSE and DNS results are each normalized so that the maximum spanwise perturbation velocity is unity. The predictions of the two methods agree very well for all perturbation components. Consequently for the DNS calculation, the principal effect of the receptivity of the flow to the simulated roughness element is the generation of a linear crossflow mode immediately downstream of the suction strip, an expected result.

Fig. 19 depicts the alignment of the crossflow vortices immediately downstream of the suction strip in the DNS calculation. The disturbances are made visible as contours of con-

stant disturbance density in a plane approximately 1.5 displacement thicknesses from the wall. By slicing Fig. 19 in a specific spanwise plane, the vortex alignment angle can be estimated on the basis of the ratio of the wavelengths in the spanwise and the streamwise directions. Whereas the dimensional spanwise wavelength is fixed, the streamwise wavelength λ_x^* varies, as shown in Fig. 20. Relative to the x axis, the vortex alignment angle is $\tan^{-1}(\alpha_r^*/\beta^*)$, where the streamwise wavenumber $\alpha_r^* = 2\pi/\lambda_x^*$. Shown in Fig. 21 are the vortex alignment angles as computed by linear stability theory (which assumes the flow to be locally parallel) and by the (nonparallel) PSE method. For comparison, the angle of the local inviscid streamline relative to the z axis is also shown. The inviscid streamline angle is derived from the boundary-layer solution as $\tan^{-1}(v_e^*/u_e^*)$. The vortex angle at $x_c = 0.2$ as derived from the DNS results is also shown and agrees closely with the PSE result. Both the DNS and PSE approaches clearly show the tendency of crossflow vortices to align nearly along inviscid streamlines. The maximum deviation in the streamline and vortex alignment angles is approximately three degrees at $x_c = 0.13$.

6 Conclusions

- Direct numerical simulation of crossflow instability in compressible flows on swept wings is computationally intensive. The simulation discussed in the previous section required 100 hours of CPU time on a Cray Y-MP, despite relatively coarse streamwise and spanwise resolution. Several factors contribute to this expense. First, long-time integration is required to established the instability. Whereas the use of implicit or semi-implicit methods of time advancement could reduce the computational expense by allowing longer time steps, such savings are not guaranteed. Joslin [16] implies that the time step needed to suppress temporal transients and numerical error is considerably less than that permitted by the stability of his semi-implicit approach. Second, because even small disturbances quickly generate a large-amplitude leading wave packet, fine grid resolution is needed to resolve nonlinearities, even if the goal is to investigate linear disturbances.

- At the present stage of development, additional effort is needed to refine both the inflow and outflow boundary conditions. It is not presently known whether the reflections experienced at the outflow boundary are physical or numerical in origin; however, given our previous experience with boundary difficulties (Pruett et al. [26]), we believe the problem can be rectified given sufficient attention.

- Despite the limitations of the numerical experiment, the qualitative and quantitative agreement between the DNS and PSE results is good. The DNS confirms that the crossflow modes predicted to be unstable by PSE are indeed unstable. Moreover, the rate of growth, the the vortex orientation angles, and the modal structures predicted by the two methods are shown to agree closely. Although more validation is warranted, particularly of strongly nonlinear interactions, we believe that, given the agreement

between the PSE and DNS methods, PSE methodology can be used reliably and inexpensively to investigate stationary crossflow instabilities on swept-wing configurations relevant to the design of the HSCT.

- An unexpected observation was the radiation of acoustic energy from the (highly nonlinear) developing wavefront as the crossflow instability was being established. Although this phenomenon is likely an artifact of the method used to generate disturbances, it underscores the capability of the DNS algorithm and suggests that the method could readily be adapted to applications in the area of aeroacoustics.

Acknowledgements

The author wishes to acknowledge the financial support of NASA and AFOSR, under contract NAS1-19656 and grant F49620-95-1-0146, respectively. The author is especially grateful to Dr. Chau-Lyan Chang for providing PSE results, to Dr. Venkit Iyer for computing the Euler solution, and to Drs. Craig Streett and Ron Joslin for wisdom and counsel in regard to the special problems encountered in simulating crossflow instability.

References

[1] D. A. Anderson, J. C. Tannehill, and R. H. Pletcher, *Computational Fluid Mechanics and Heat Transfer*, Taylor and Francis, New York, 1984, pp. 220, 396-398.

[2] F. Bertolotti and Th. Herbert, "Analysis of the Linear Stability of Compressible Boundary Layers Using the PSE," *Theoret. Comput. Fluid Dynamics*, Vol. 3, No. 2, 1991, pp. 117-124.

[3] L. N. Cattafesta III, V. Iyer, J. A. Masad, R. A. King, and J. R. Dagenhart, "Three-Dimensional Boundary-Layer Transition on a Swept Wing at Mach 3.5," AIAA Paper No. 94-2375, 1994.

[4] C.-L. Chang, M. R. Malik, M. Y. Hussaini, and G. Erlebacher, "Compressible Stability of Growing Boundary Layers Using Parabolized Stability Equations," AIAA Paper No. 91-1636, 1991.

[5] C.-L. Chang, "ECLIPSE: An Efficient Compressible Linear PSE Code for Swept-Wing Boundary Layers," High Technology Report No. HTC-9503, 1995.

[6] C.-L. Chang, M. R. Malik, and H. Vinh, "Linear and Nonlinear Stability of Compressible Swept-Wing Boundary Layers," AIAA Paper 95-2278, 1995.

[7] C.-L. Chang and M. R. Malik, "Non-parallel Stability of Compressible Boundary Layers," AIAA Paper No. 93-2912, 1993.

[8] C.-L. Chang, personal communication, 1995.

[9] M. M. Choudhari, "Roughness-Induced Generation of Crossflow Vortices in Three-Dimensional Boundary Layers," *Theoret. Comput. Fluid Dynamics*, Vol. 6, No. 1, 1994, pp. 1-30.

[10] M. M. Choudhari and C. L. Streett, AIAA Paper No. 90-5258, 1990.

[11] D. A. Fuciarelli and H. L. Reed, "Stationary Crossflow Vortices," *Phys. Fluids A*, Vol. 4, No. 9, 1992, p. 1880.

[12] P. Hall, "The Goertler Vortex Instability Mechanism in Three-Dimensional Boundary Layers," *Proc. R. Soc. London Ser. A*, Vol. 399, 1985, pp. 135-152.

[13] C.-M. Ho and Y.-C. Tai, "Manipulating Boundary-Layer Flow with Micromach-Based Sensors and Actuators," presented at the 12th U.S. National Congress of Applied Mechanics, Seattle, Washington, June 27-July 1, 1994.

[14] V. S. Iyer, personal communication, 1994.

[15] V. S. Iyer, R. Spall, and J. Dagenhart, "Computational Study of Transition Front on a Swept Wing Leading-Edge Model," *J. of Aircraft*, Vol. 31, No. 1, 1994.

[16] R. D. Joslin, "Evolution of Stationary Crossflow Vortices in Boundary Layers on Swept Wings," *AIAA J.*, Vol. 33, No. 7, 1995, pp 1279-1285.

[17] R. D. Joslin, "Direct Simulation of Evolution and Control of Three-Dimensional Instabilities in Attachment-Line Boundary Layers," *J. Fluid Mech.*, Vol. 291, 1995, pp. 369-392.

[18] R. D. Joslin and C. L. Streett, "The Role of Stationary Crossflow Vortices in Boundary-Layer Transition on Swept Wings," *Phys. Fluids A*, Vol. 6, No. 10, 1994, pp. 3442-3453.

[19] R.-S. Lin and H. L. Reed, "Navier-Stokes Simulation of Stationary Crossflow Vortices on a Swept Wing," *Bulletin of the American Physical Society*, Vol. 36, No. 10, 1991, p. 2631.

[20] L. M. Mack, "Boundary-Layer Stability Theory," in *Special Course on Stability and Transition of Laminar Flow*, ed. R. Michel, AGARD Report No. 709, 1984, pp. 3.1-3.81.

[21] M. R. Malik, F. Li, and C.-L. Chang, "Crossflow Disturbances in Three-Dimensional Boundary Layers," *J. Fluid Mech.*, Vol. 268, 1994, pp. 1-36.

[22] T. J. Poinsot and S. K. Lele, "Boundary Conditions for Direct Simulations of Compressible Viscous Flows," *J. Comput. Phys.*, Vol. 101, 1992, pp. 104-129.

[23] C. D. Pruett and Craig L. Streett, "A Spectral Collocation Method for Compressible, Non-similar Boundary Layers," *Int. J. Numer. Meth. Fluids*, Vol. 13, No. 6, 1991, pp. 713-737.

[24] C. D. Pruett, "On the Accurate Prediction of the Wall-Normal Velocity in Compressible Boundary-Layer Flow," *Int. J. Numer. Meth. Fluids*, Vol. 16, 1993, pp. 133-152.

[25] C. D. Pruett, "A Spectrally Accurate Boundary-Layer Code for Infinite Swept Wings," NASA Contractor Report 195014, 1994.

[26] C. D. Pruett, T. A. Zang, C.-L. Chang, and M. H. Carpenter, "Spatial Direct Numerical Simulation of High-Speed Boundary-Layer Flows–Part I: Algorithmic Considerations and Validation," *Theoret. Comput. Fluid Dynamics*, Vol. 7, No. 1, 1995, pp. 49-76.

[27] C. D. Pruett and C.-L. Chang, "Spatial Direct Numerical Simulation of High-Speed Boundary-Layer Flows–Part II: Transition on a Cone in Mach 8 Flow," *Theoret. Comput. Fluid Dynamics*, to appear.

[28] Helen L. Reed and William S. Saric, "Stability of Three-Dimensional Boundary Layers," *Annu. Rev. Fluid. Mech*, Vol. 21, 1989, pp. 235-284.

[29] C. L. Streett and M. G. Macaraeg, "Spectral Multi-Domain for Large-Scale Fluid Dynamic Simulations," *Appl. Numer. Math*, Vol. 6, 1989/90, pp. 123-139.

[30] J. H. Williamson, "Low-Storage Runge-Kutta Schemes," *J. Comput. Phys.*, Vol. 35, 1980, pp. 48-56.

Figures

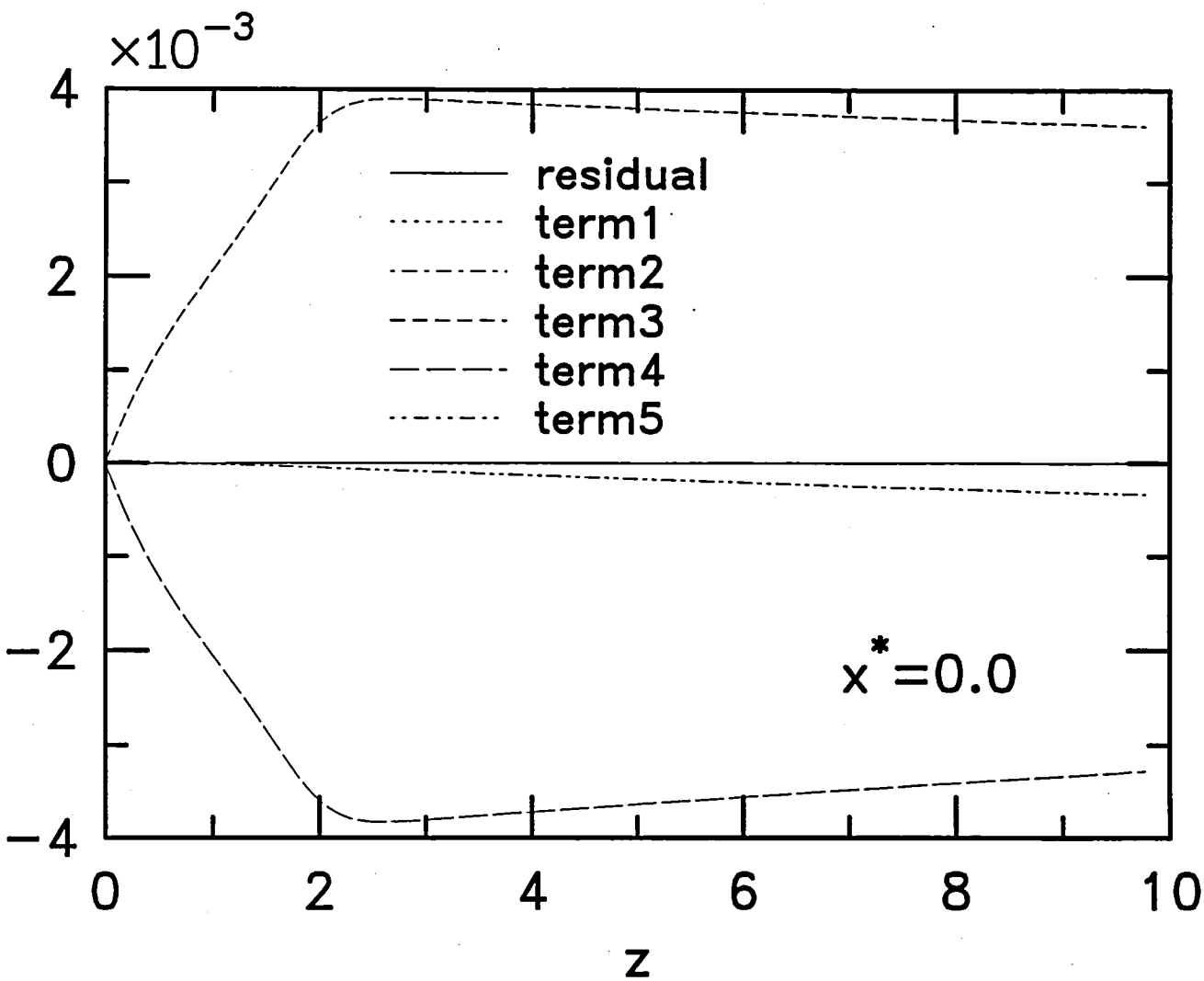

1. Individual terms of continuity equation and total residual at attachment line.

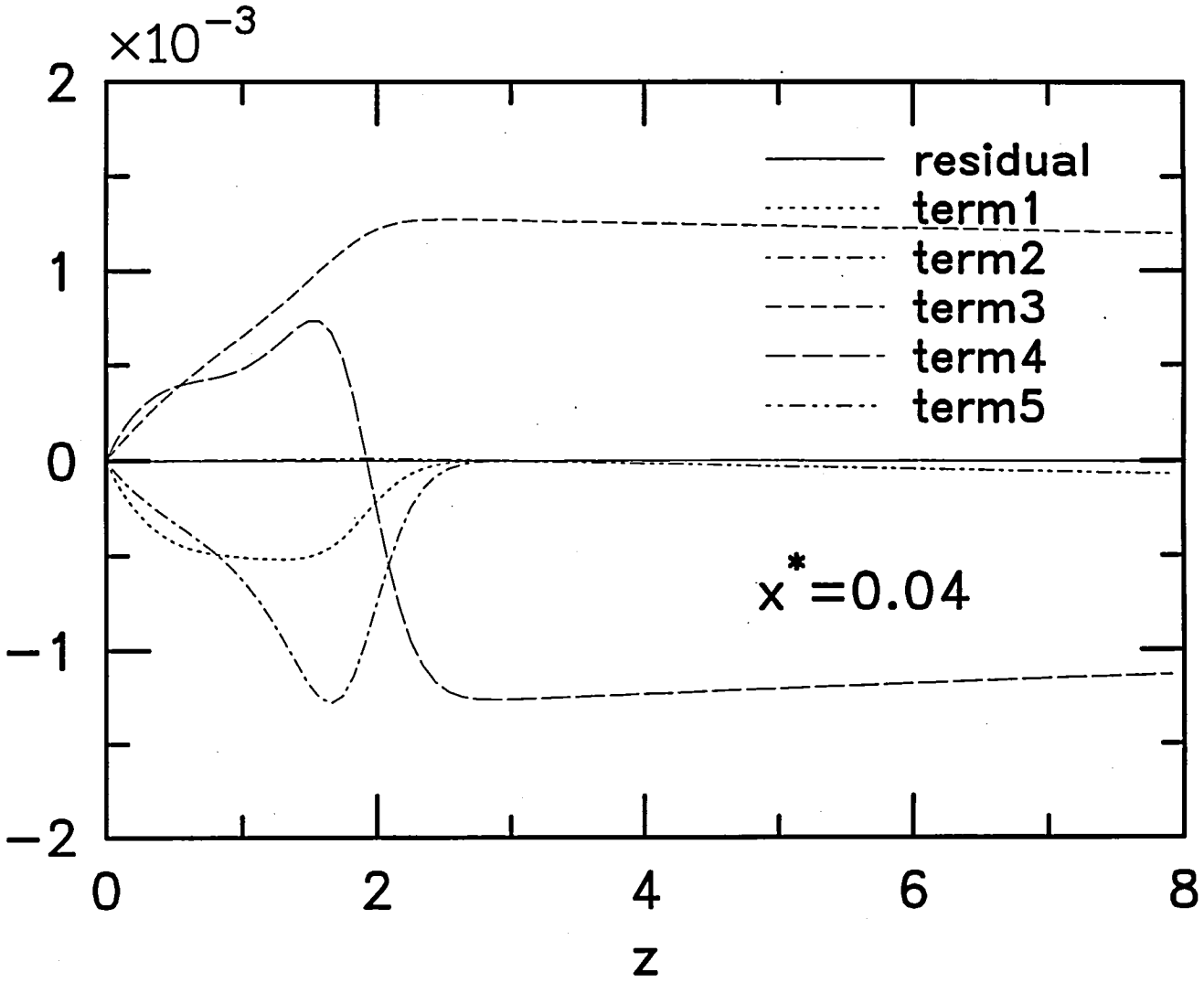

2. Individual terms of continuity equation and total residual at $x^* = 0.04$ ft.

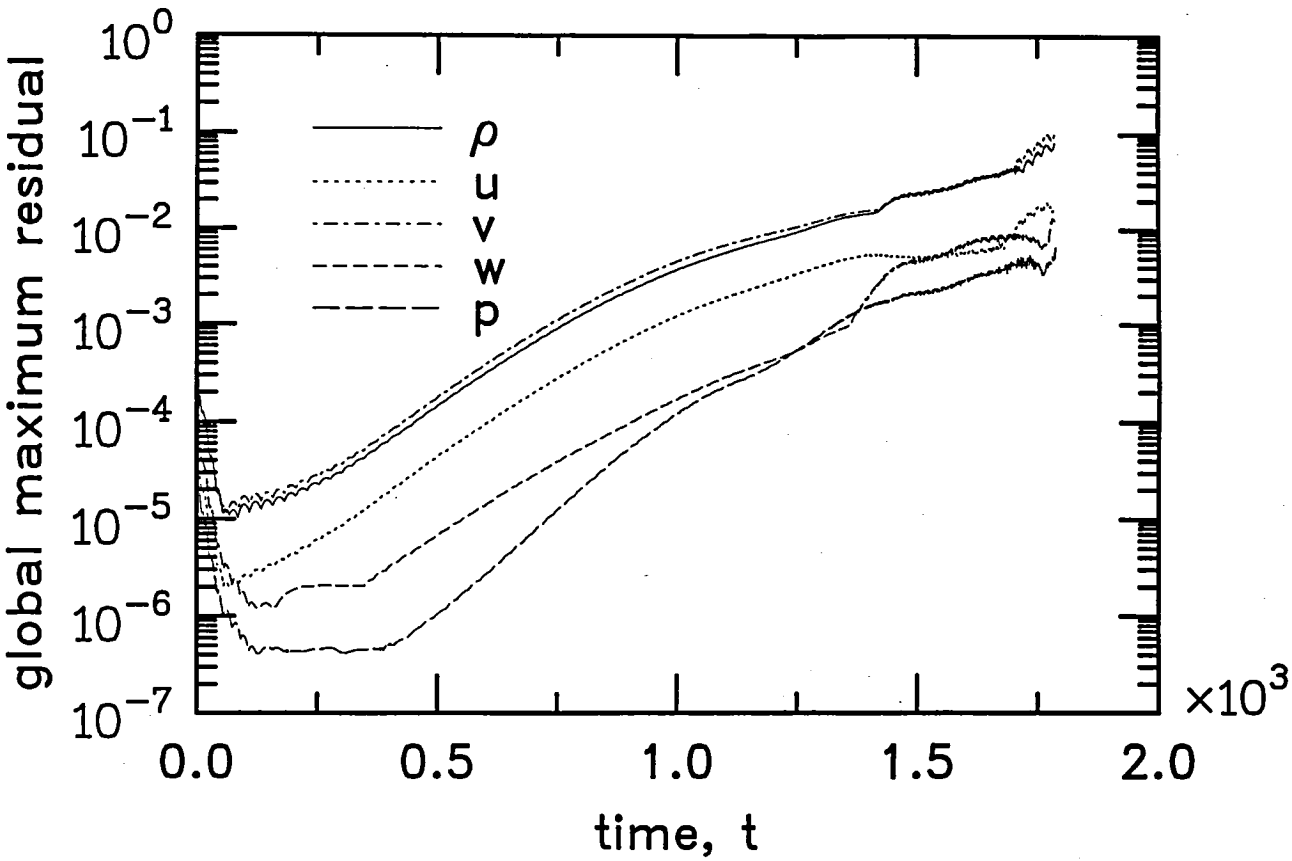

3. Temporal evolution of global maximum residuals of time-independent compressible Navier-Stokes equations.

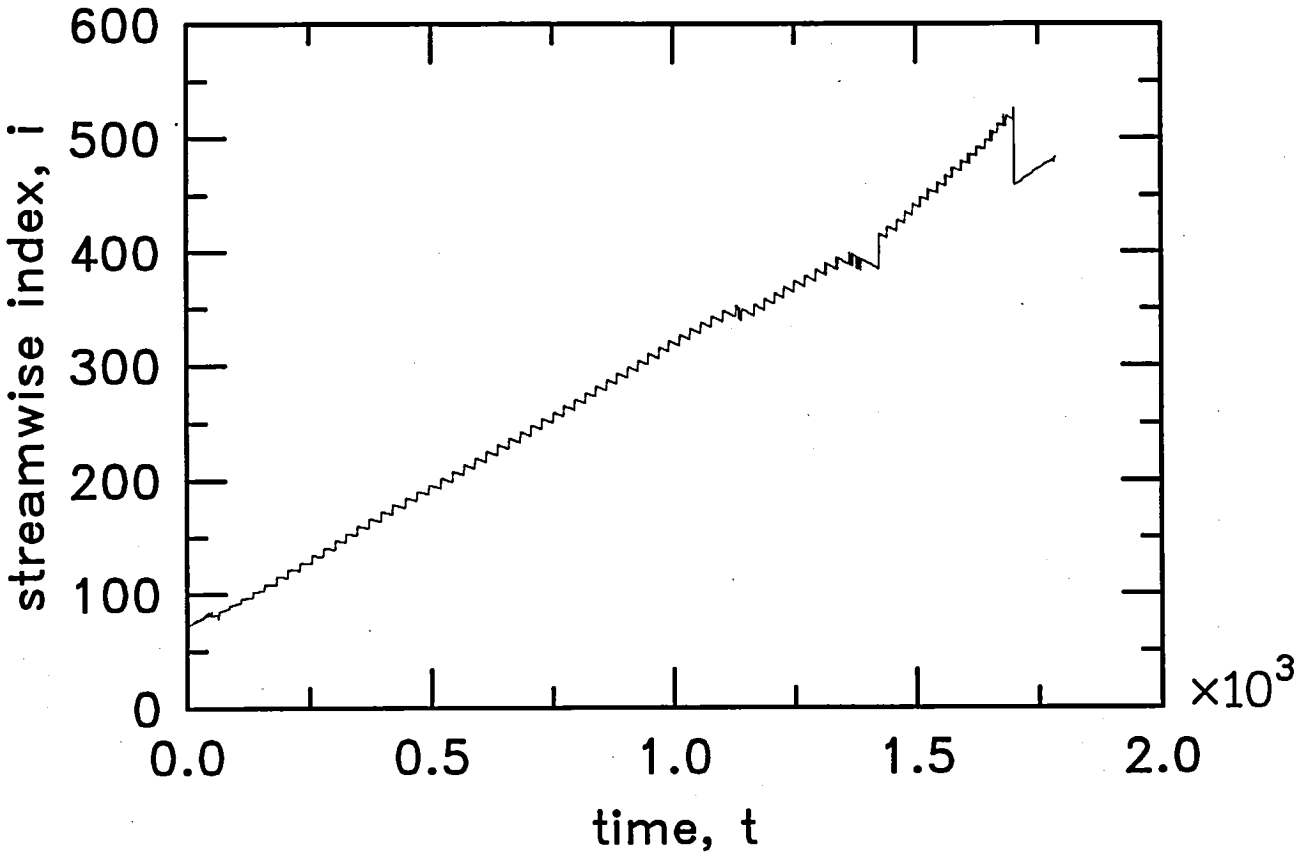

4. Streamwise index of global maximum residual versus time.

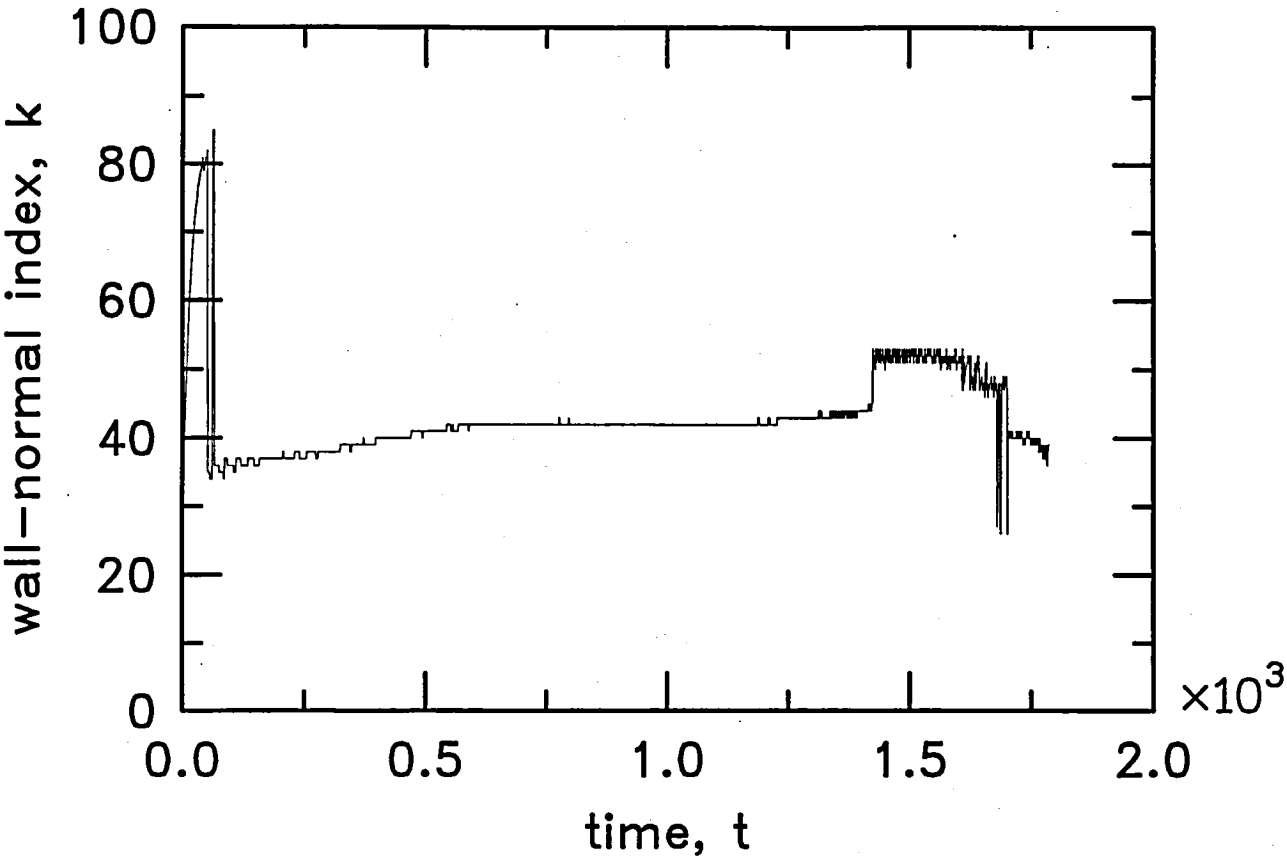

5. Wall-normal index of global maximum residual versus time.

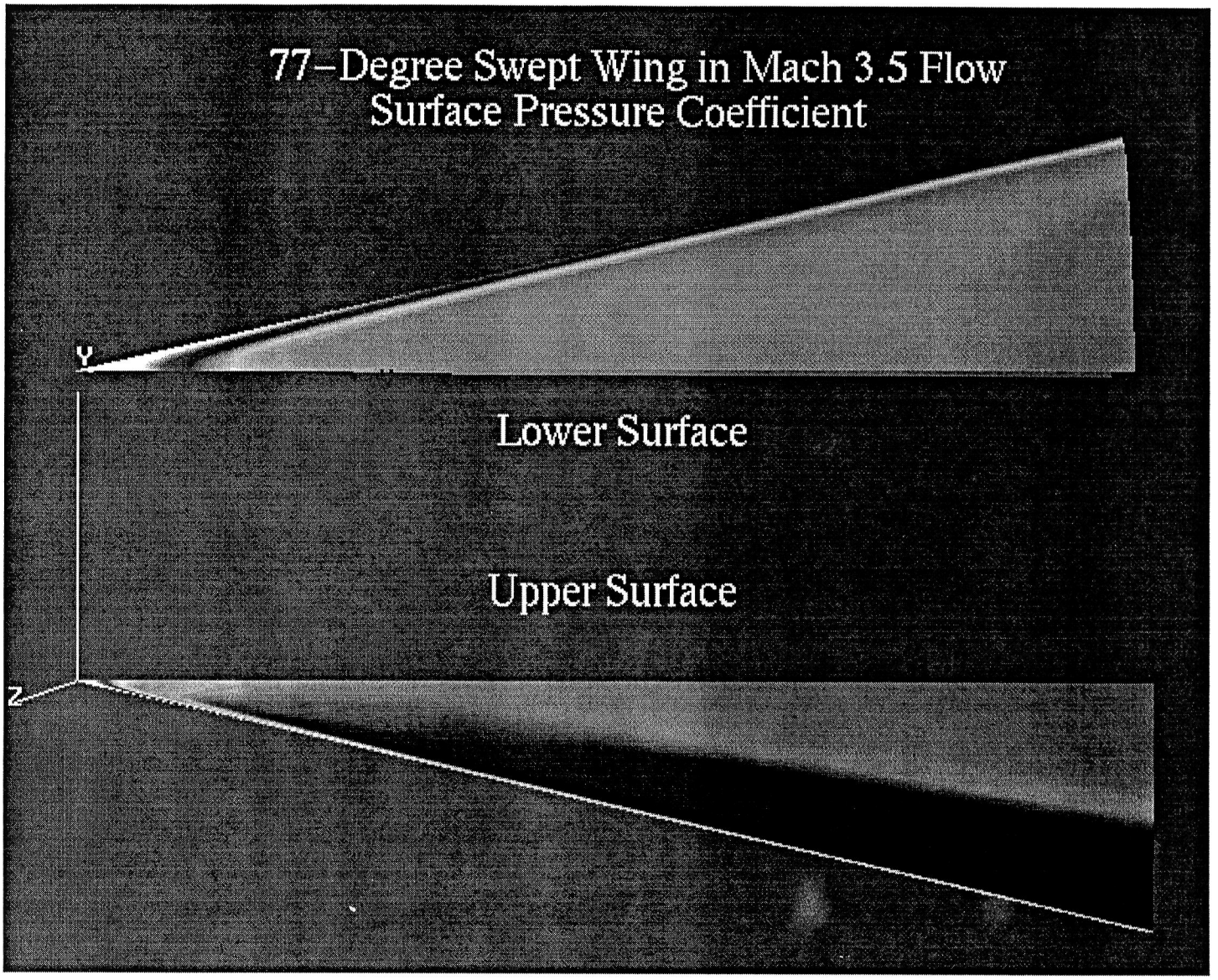

6. Euler solution displaying isobars of constant pressure on upper and lower surfaces of wing model of Cattafesta et al. [3]

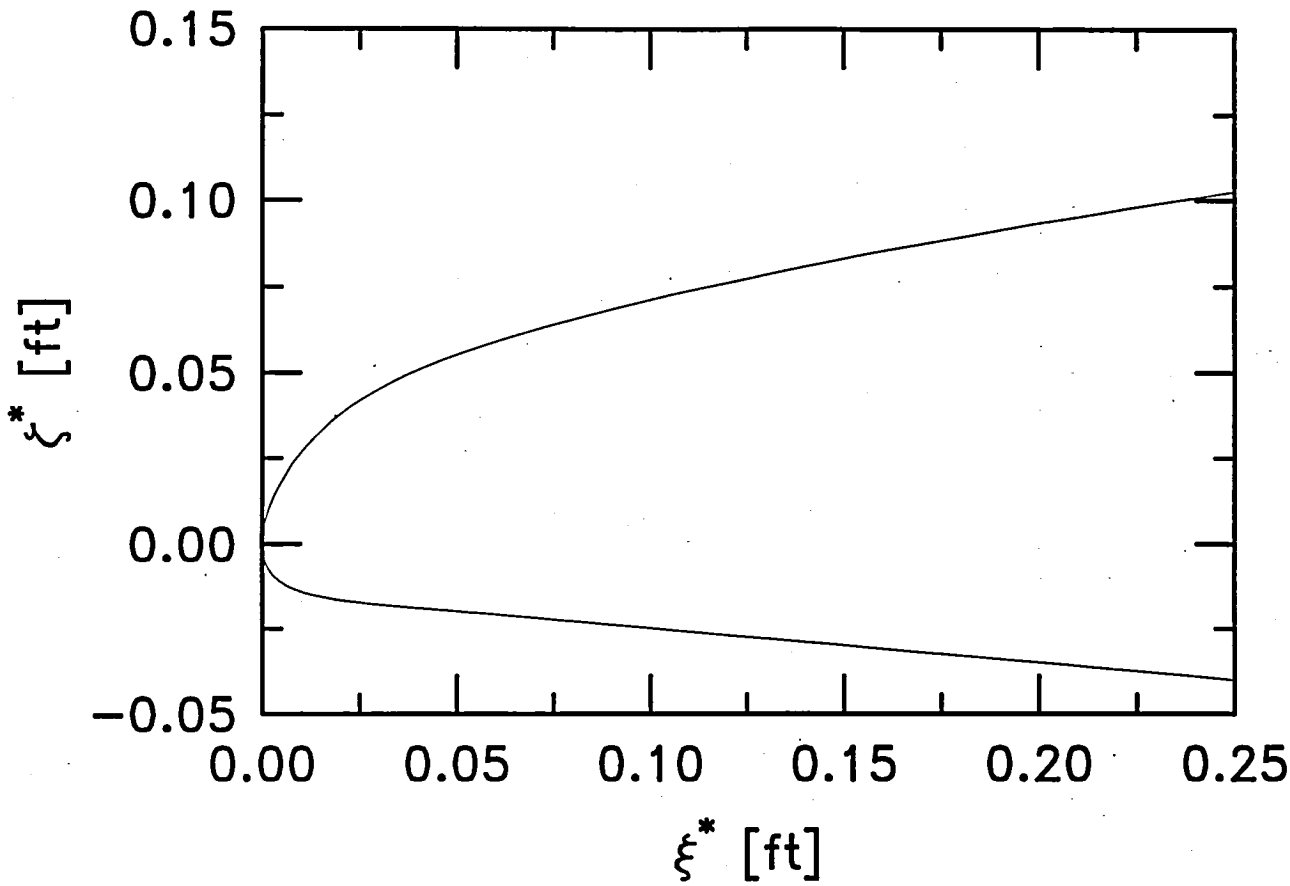

7. Wing section perpendicular to leading edge.

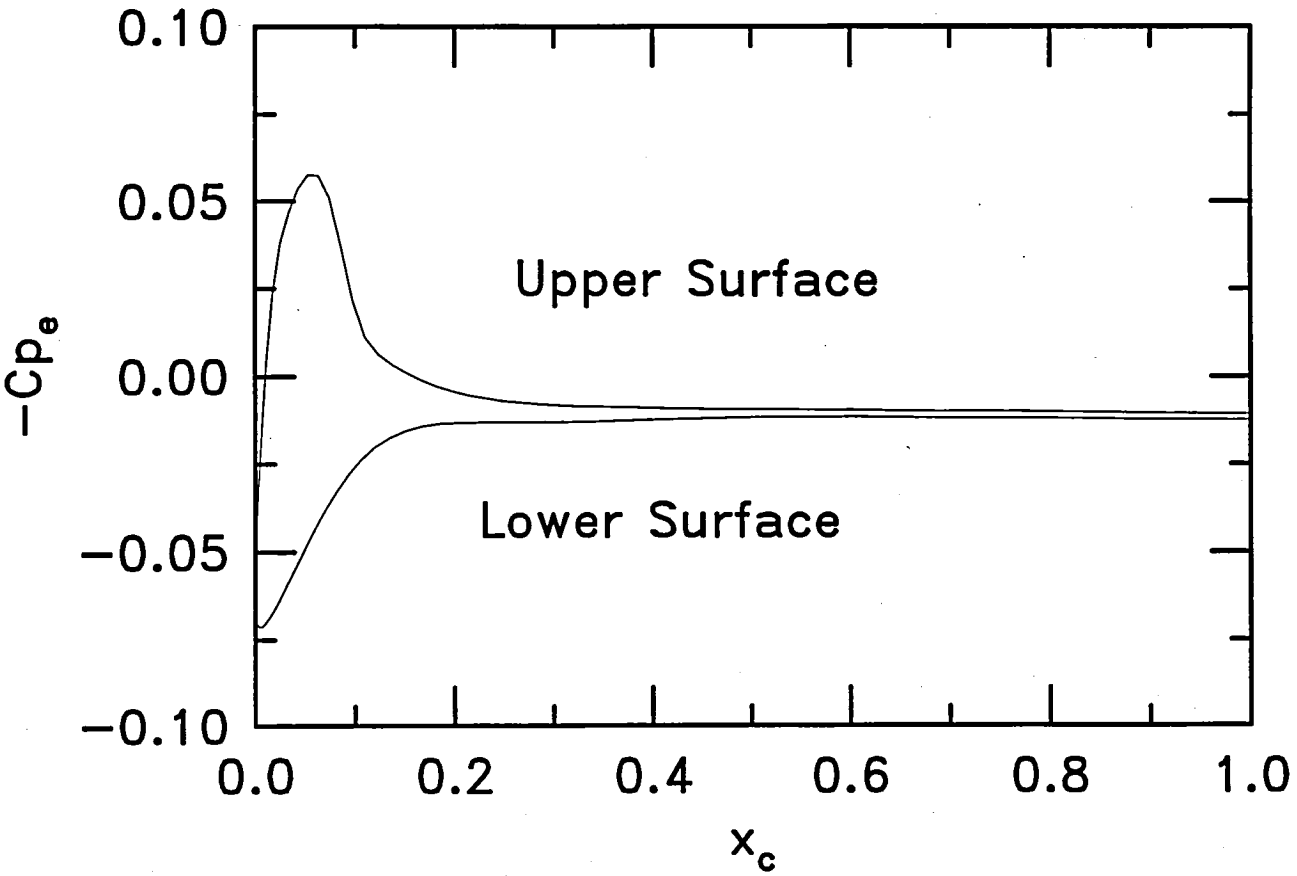

8. Surface pressure coefficients for wing section of Fig. 7.

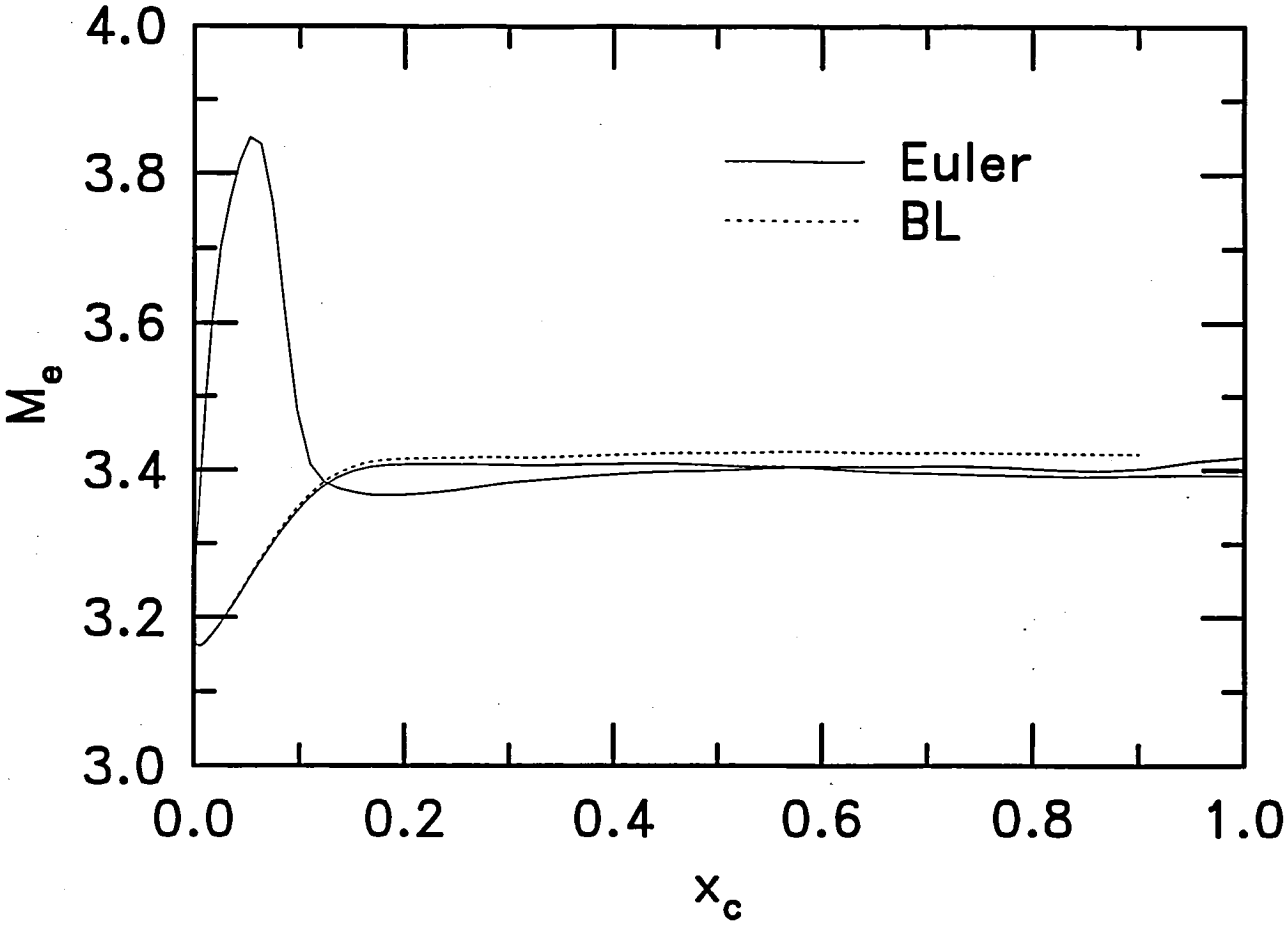

9. Edge Mach-number distribution for wing section of Fig. 7.

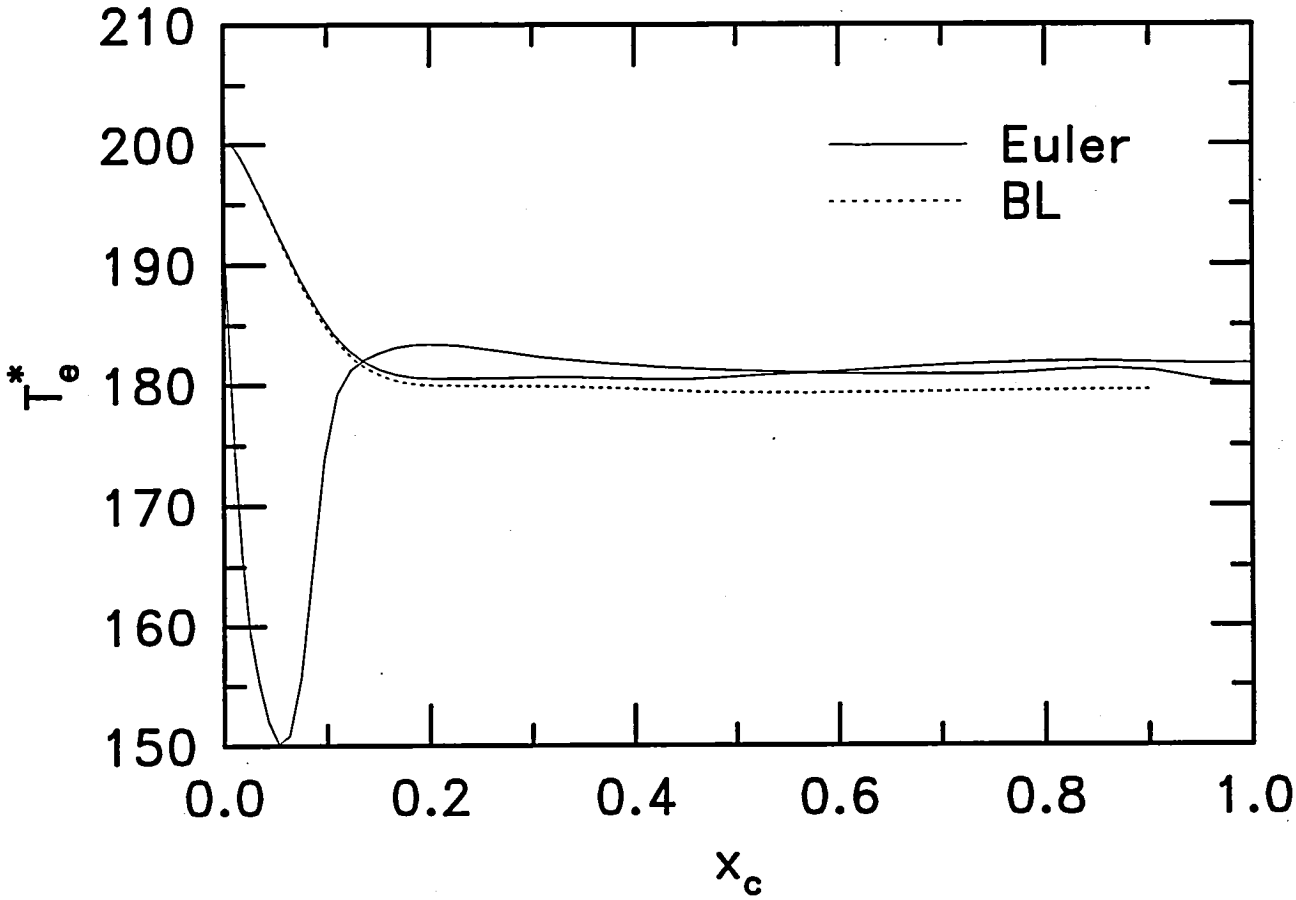

10. Edge temperature distribution for wing section of Fig. 7.

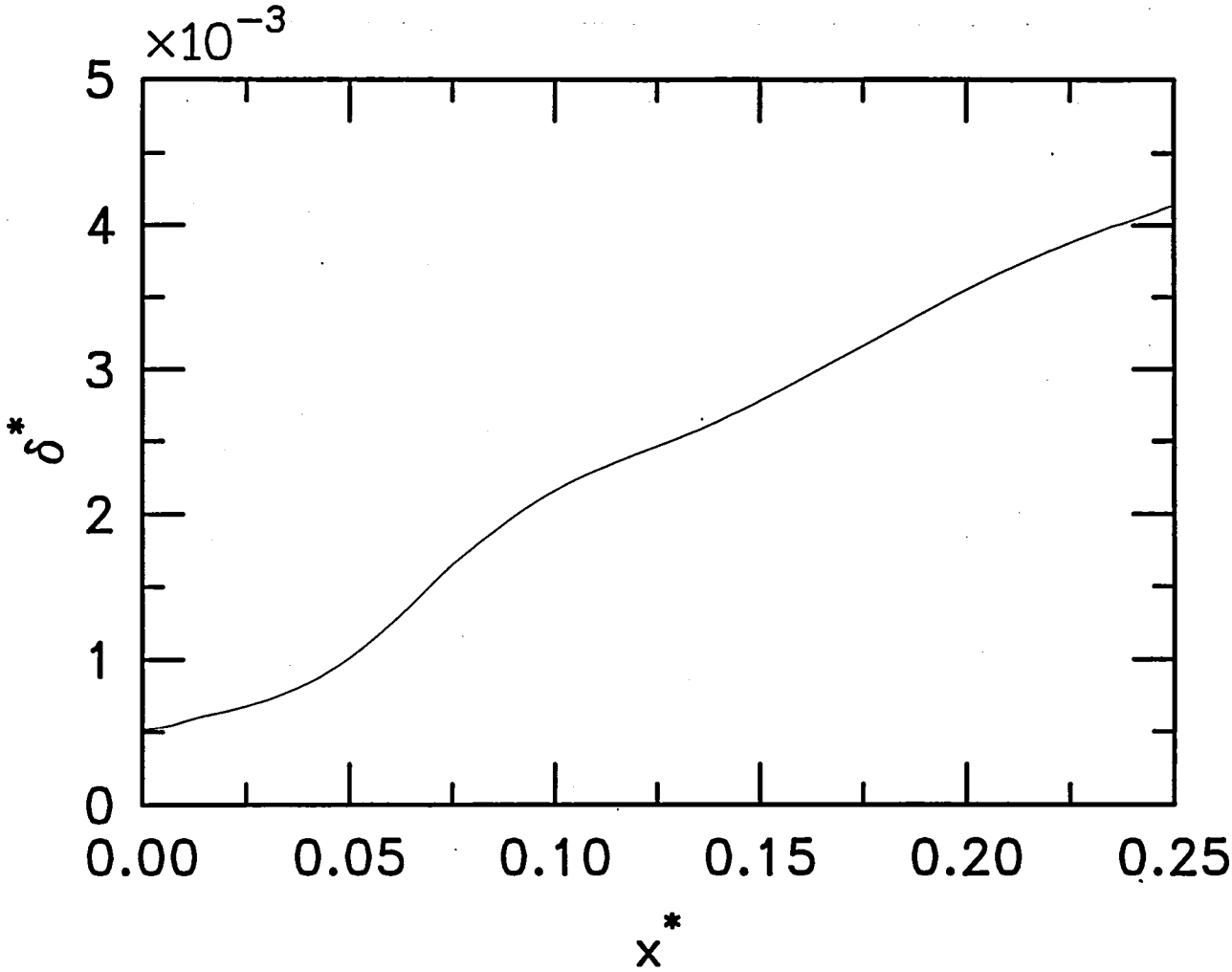

11. Evolution of boundary-layer displacement thickness on upper surface of wing section of Fig. 7.

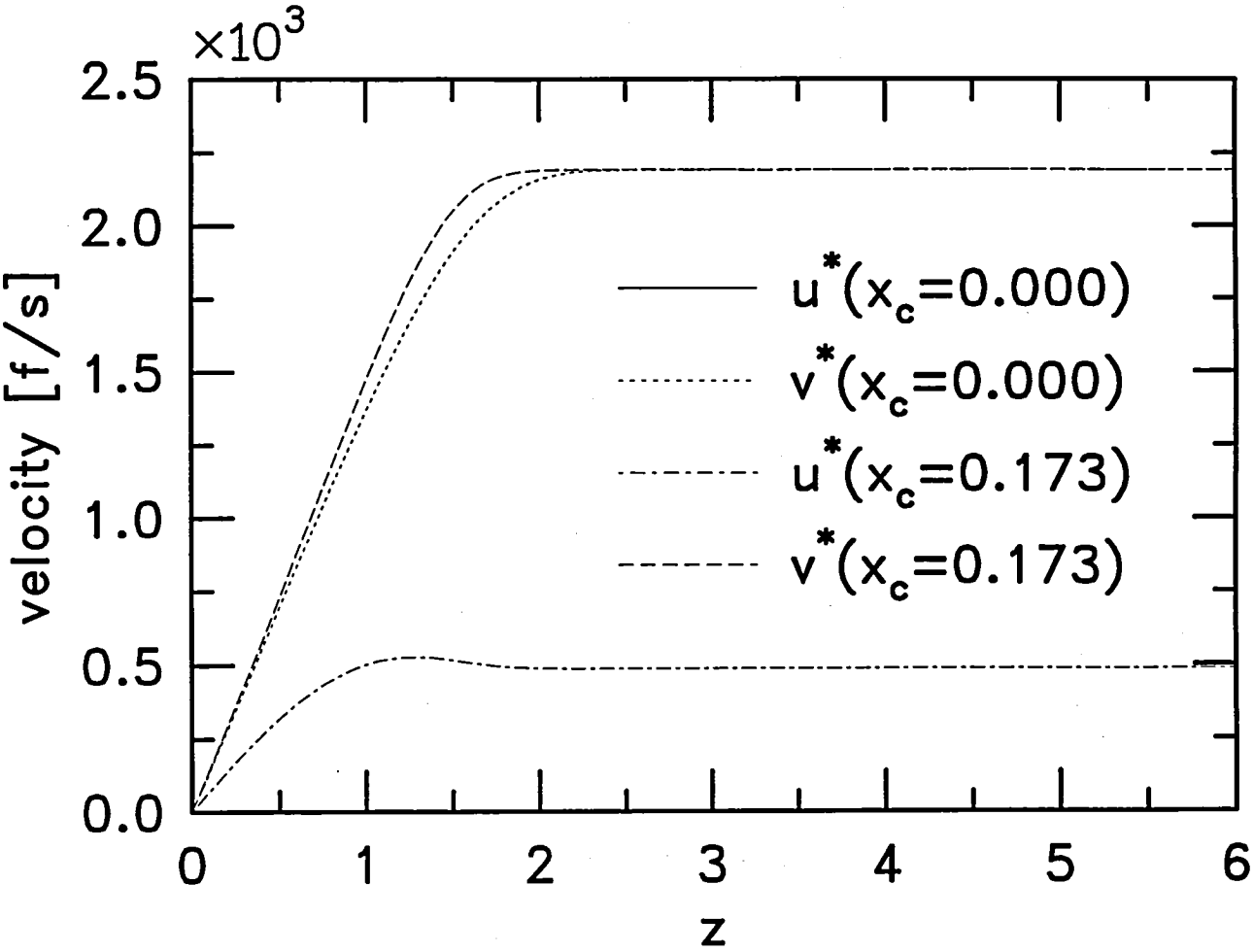

12. Wall-normal distributions of streamwise and spanwise velocities at attachment line and at $x_c = 0.173$ on upper wing surface.

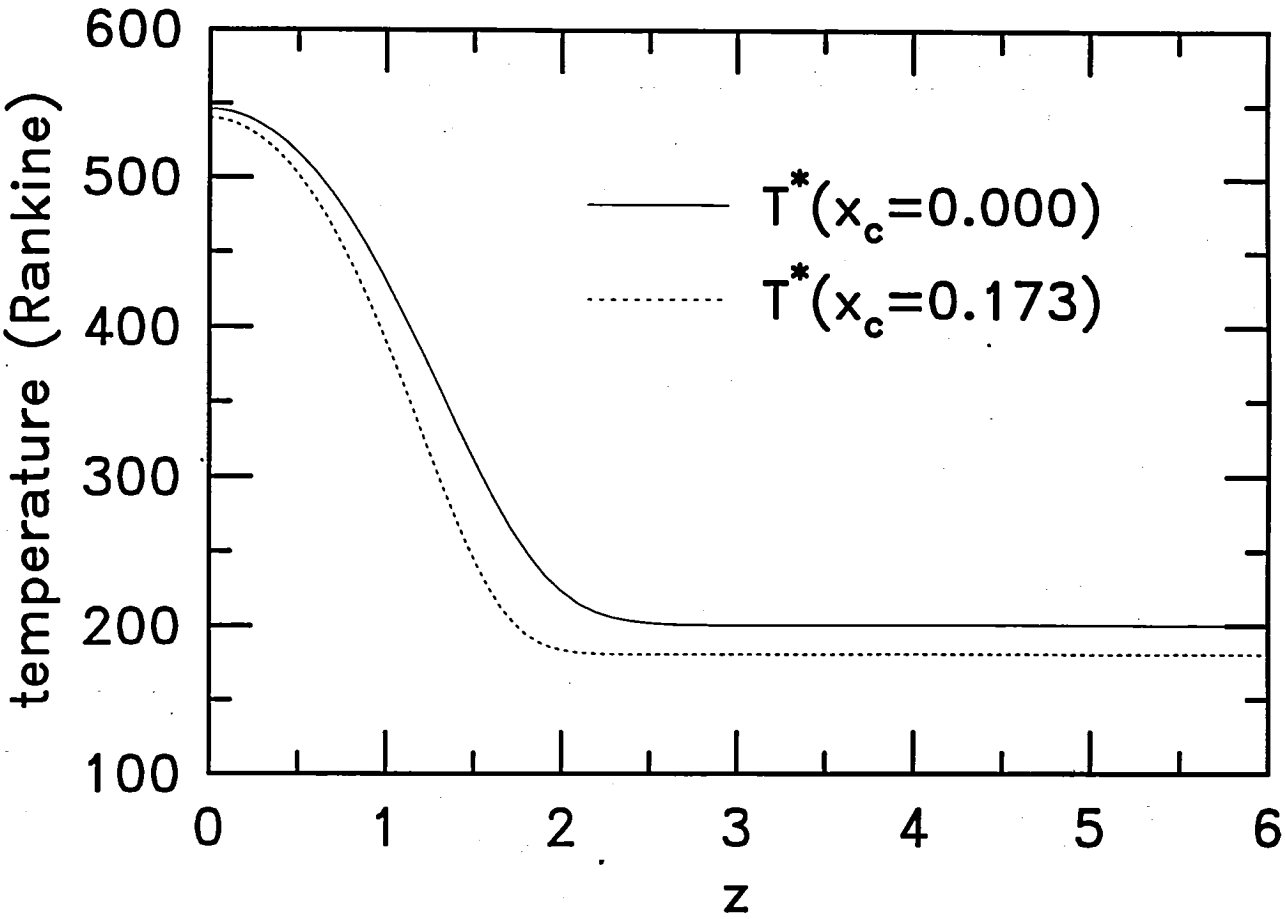

13. Wall-normal distribution of temperature at attachment line and at $x_c = 0.173$.

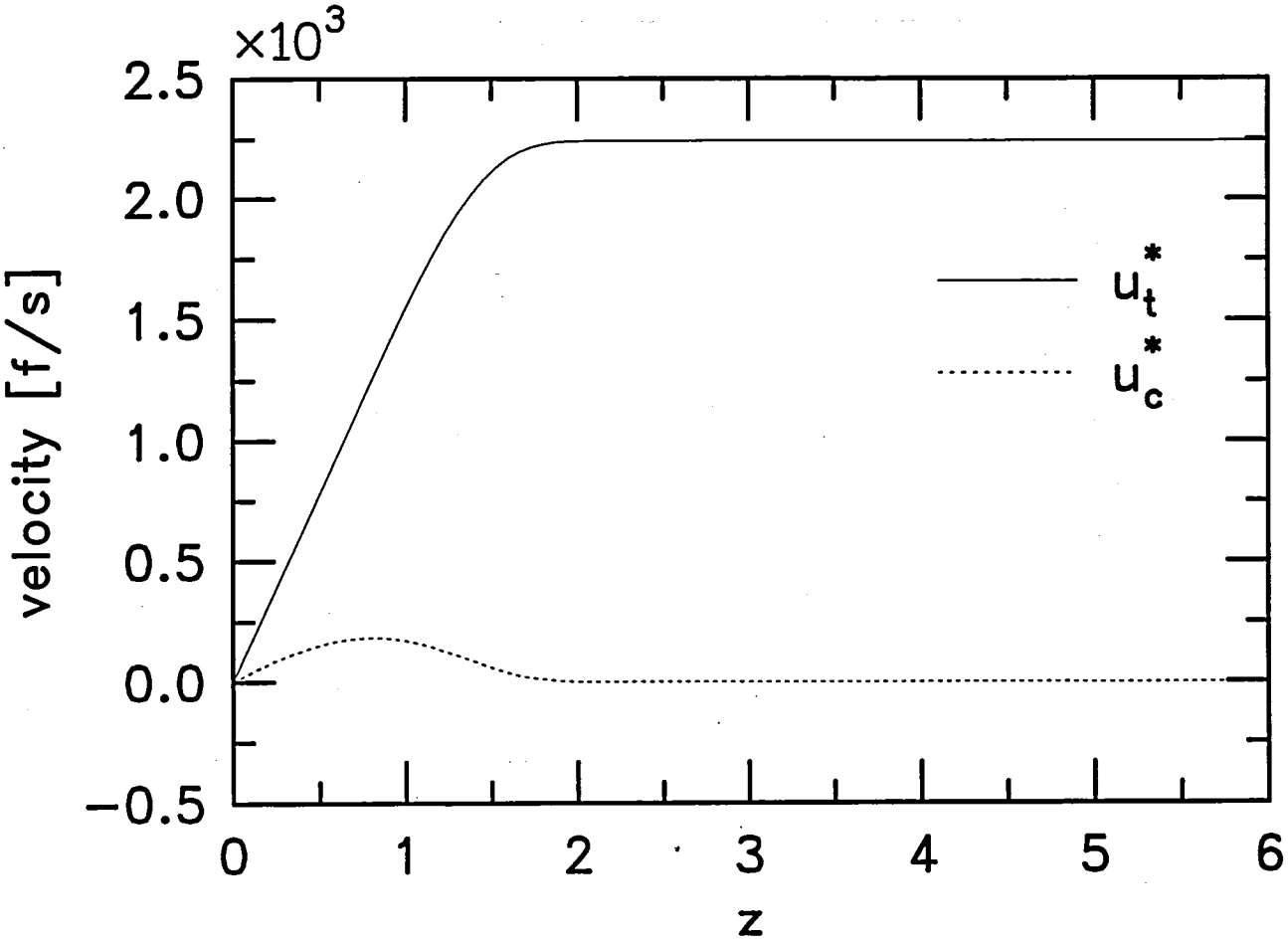

14. Comparison of tangential and crossflow velocities at $x_c = 0.173$ on upper wing surface.

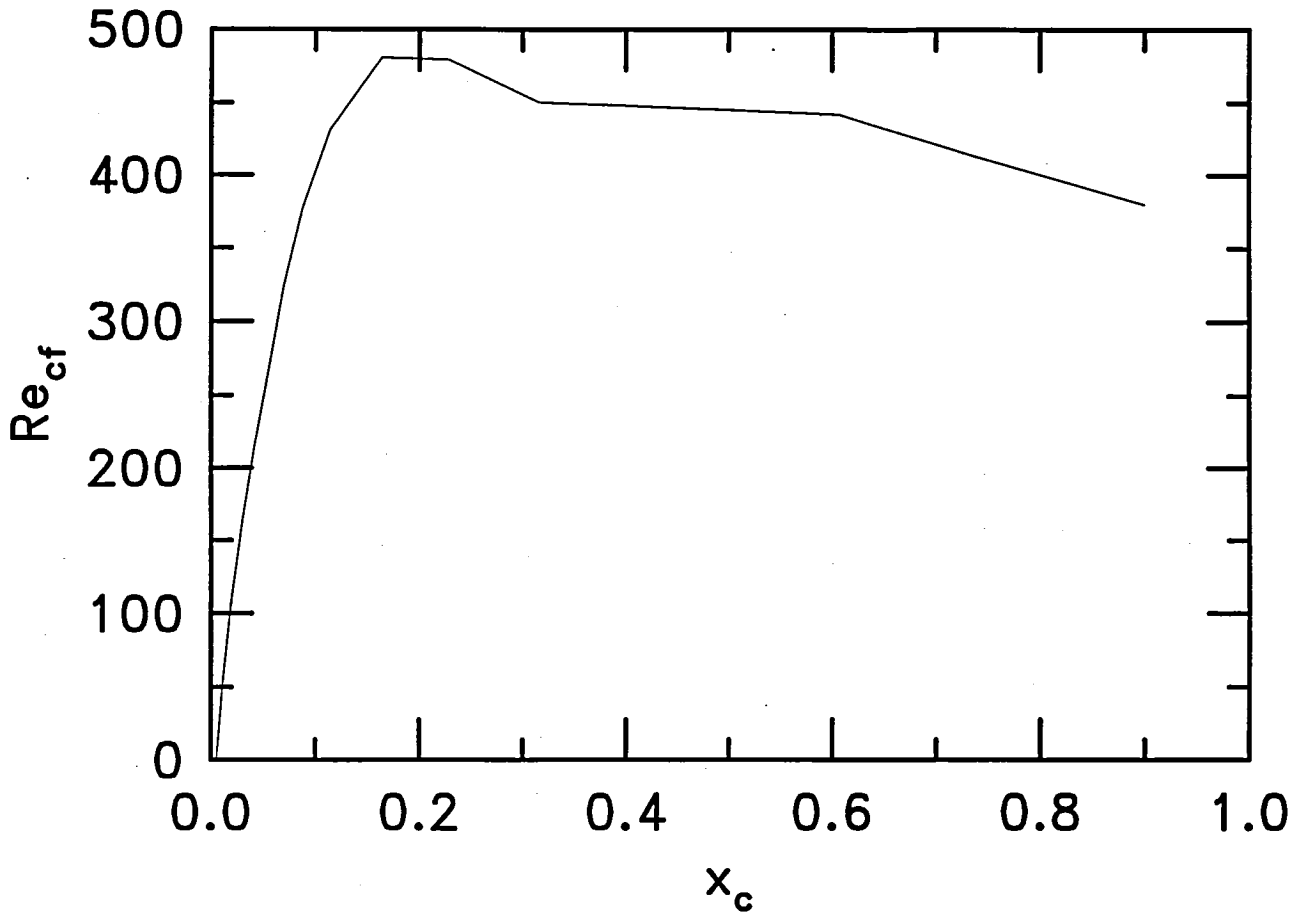

15. Streamwise evolution of crossflow Reynolds number on upper wing surface.

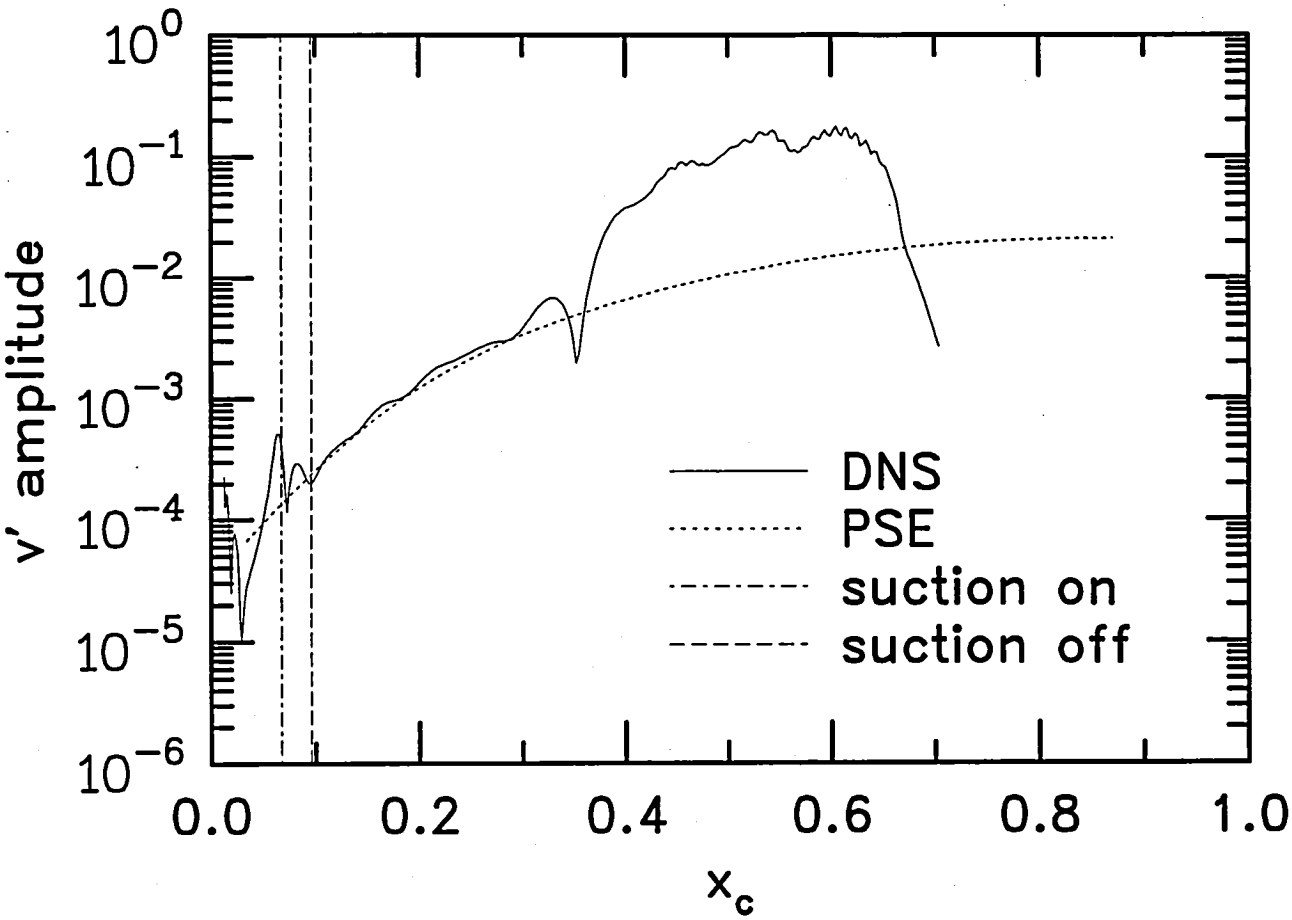

16. Streamwise evolution of maximum of fundamental of spanwise velocity perturbation.

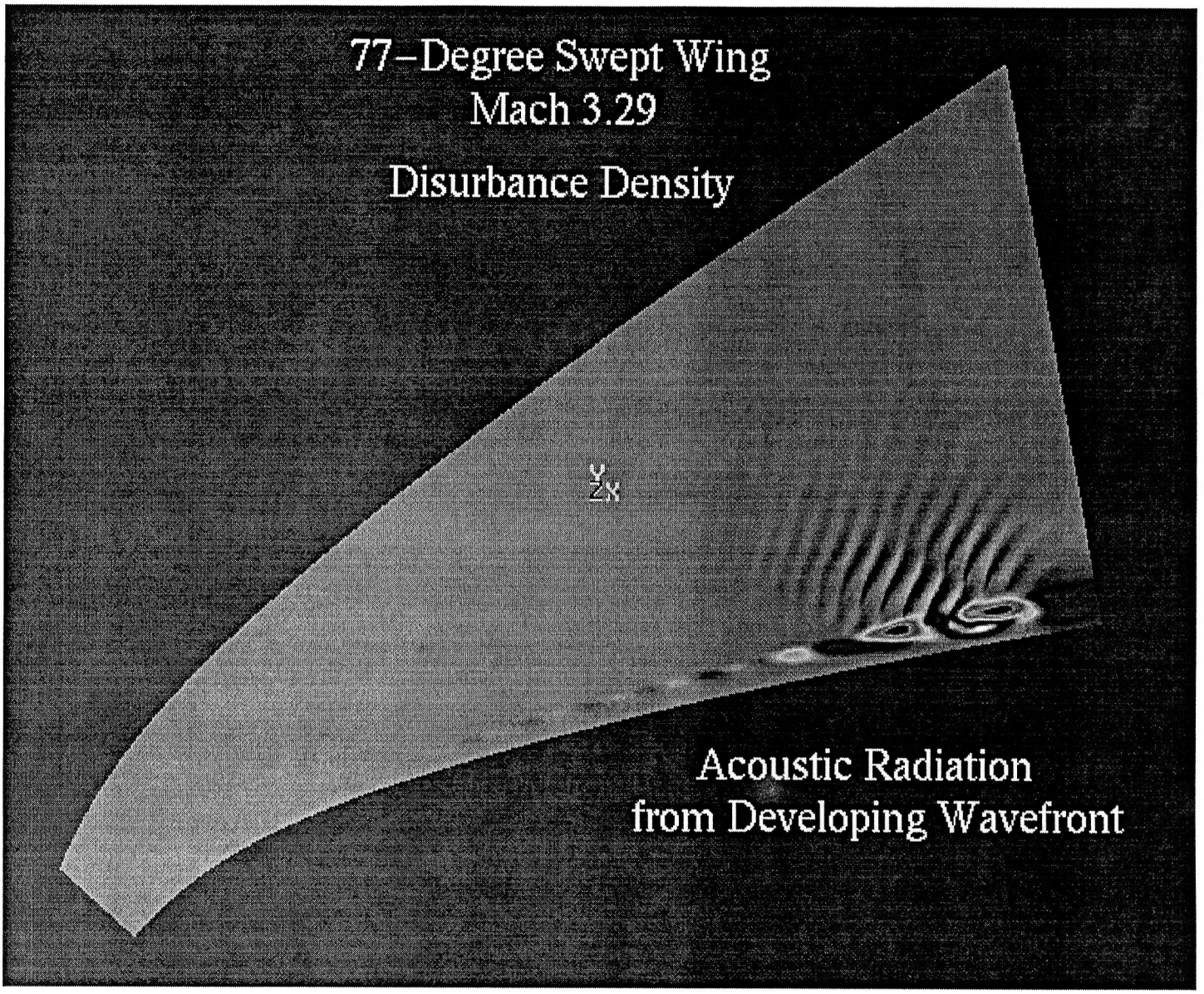

17. Contours of constant disturbance density in computational plane normal to both leading edge and wing surface showing acoustic energy generated by strong nonlinearity in wave-packet region.

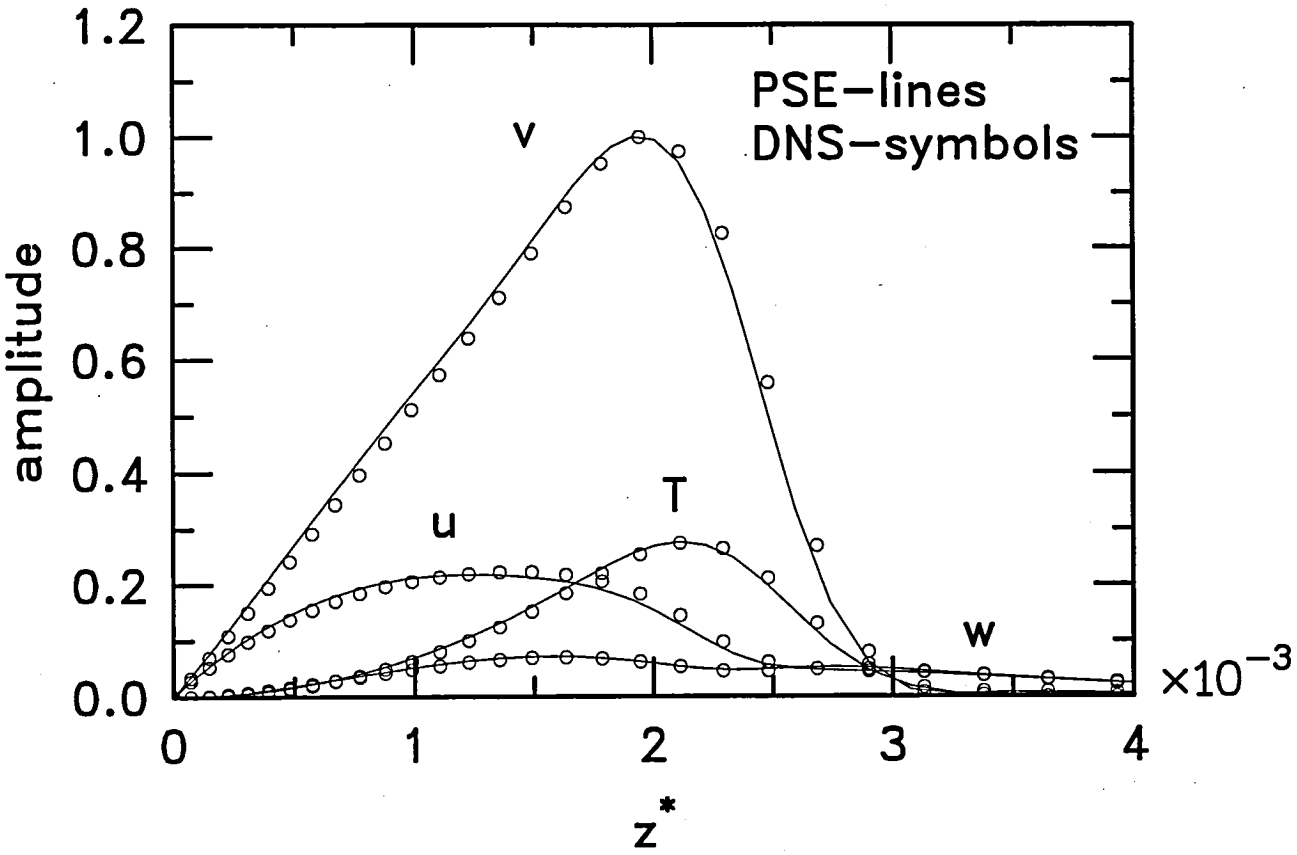

18. Comparison of amplitude distributions of components of fundamental spanwise Fourier component of DNS calculation with PSE-derived crossflow disturbance at $x_c = 0.22$. In each case, results are normalized so that maximum spanwise perturbation velocity is unity. (Even indexed DNS values omitted.)

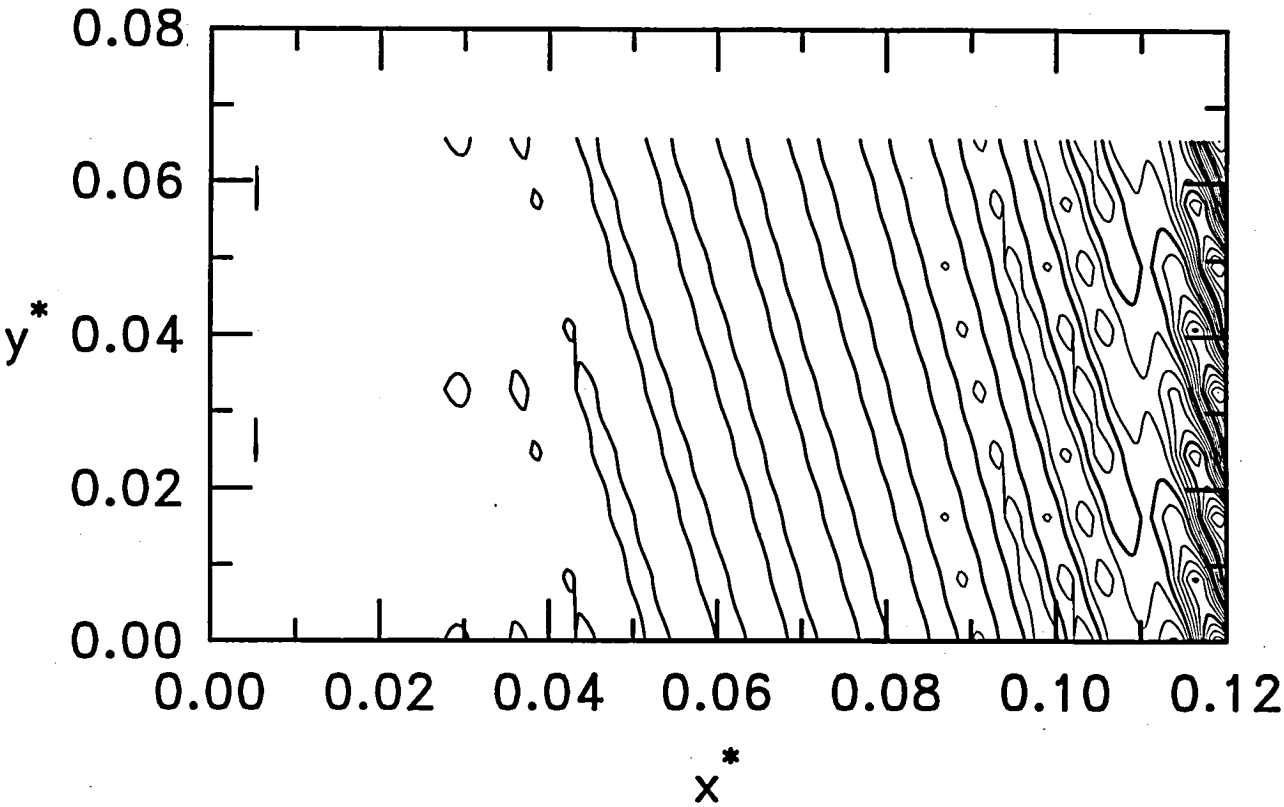

19. Contours of constant perturbation density in surface approximately 1.5 displacement thicknesses from wall showing alignment of crossflow vortices. Computational domain is replicated once in span for aesthetics.

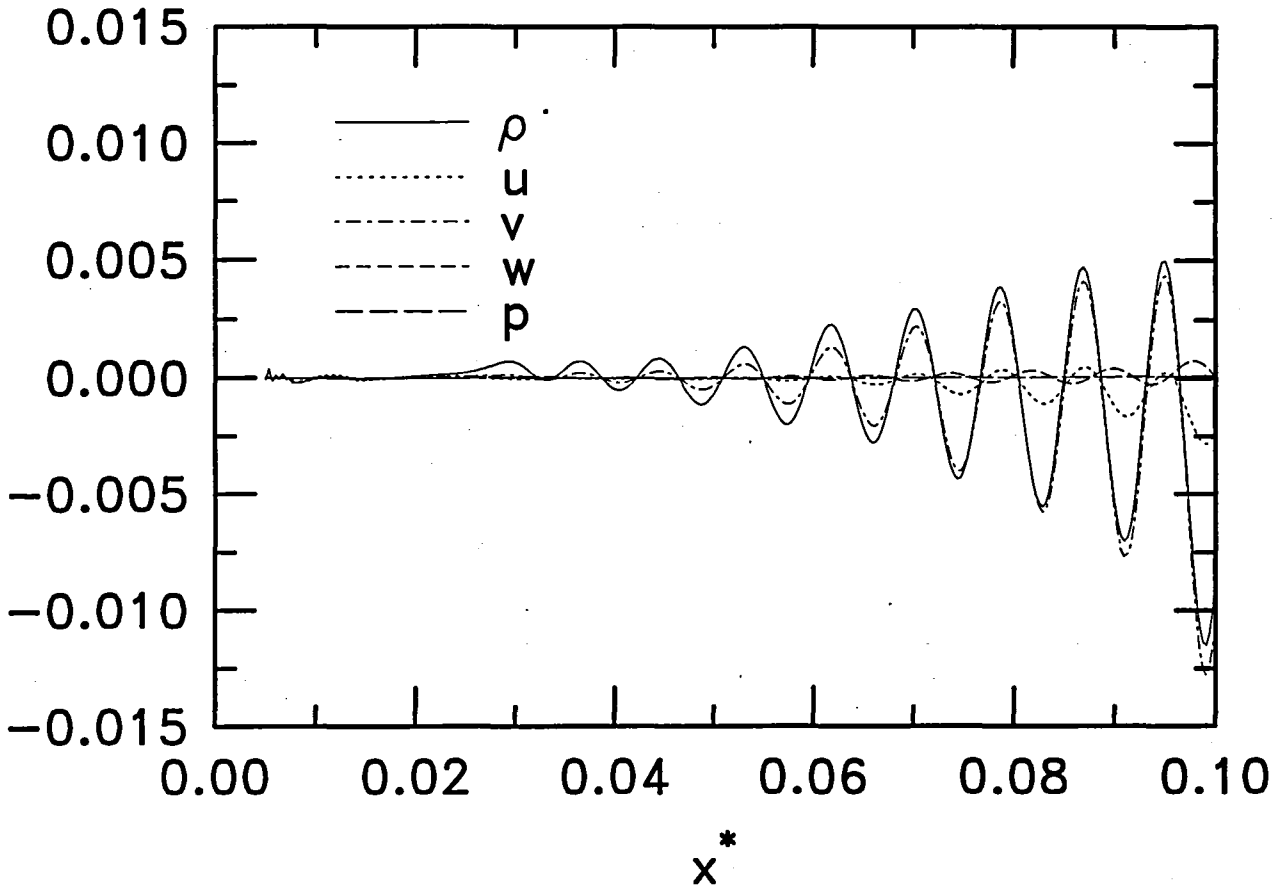

20. Projection of perturbation density field of Fig. 19 onto selected spanwise plane showing streamwise wavelength of dominant crossflow mode.

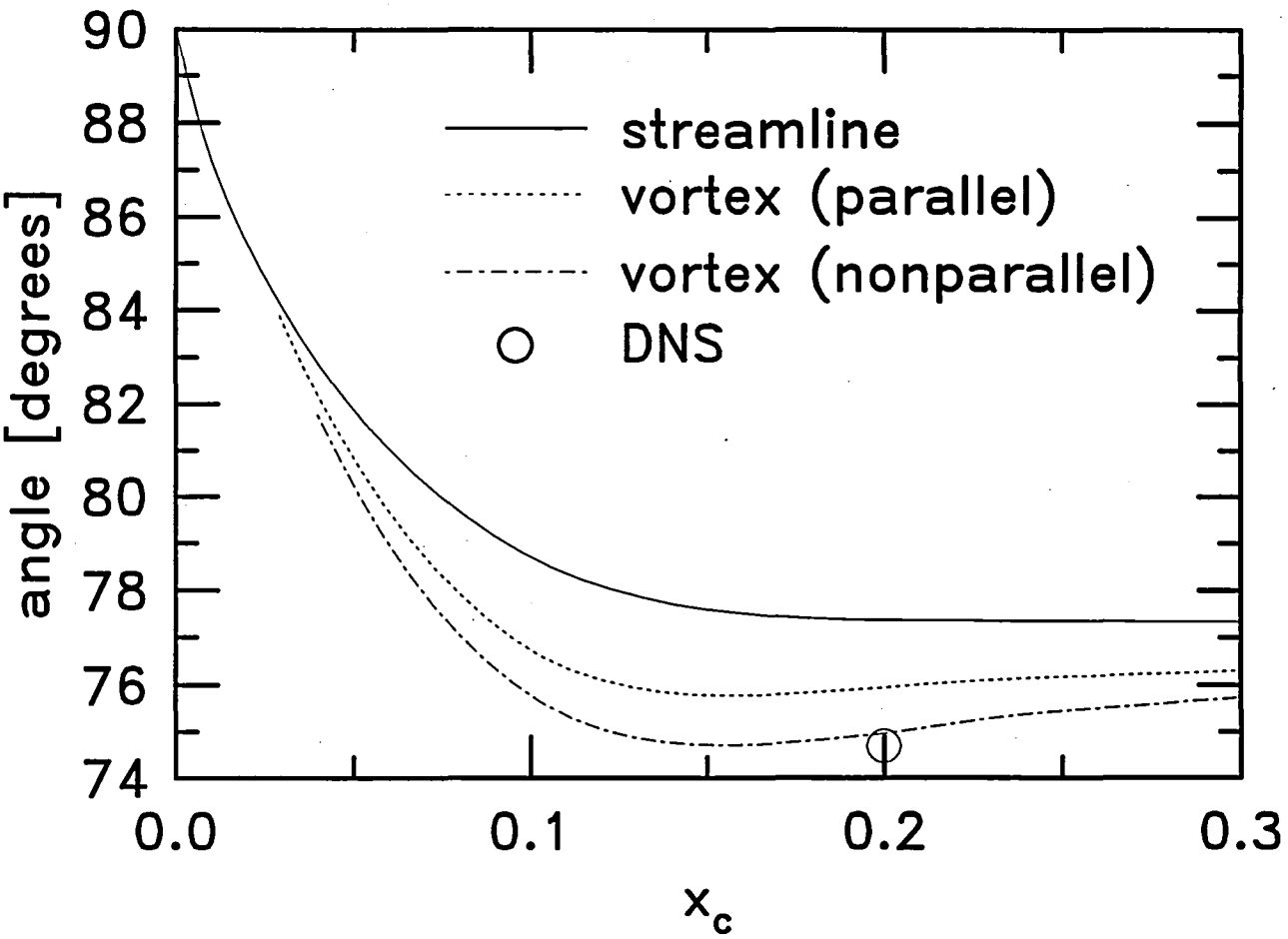

21. Comparison of vortex-alignment angle and inviscid-streamline angle relative to x-axis showing orientation of crossflow mode in direction of inviscid streamlines.

REPORT DOCUMENTATION PAGE

Form Approved
OMB No. 0704-0188

Public reporting burden for this collection of information is estimated to average 1 hour per response, including the time for reviewing instructions, searching existing data sources, gathering and maintaining the data needed, and completing and reviewing the collection of information. Send comments regarding this burden estimate or any other aspect of this collection of information, including suggestions for reducing this burden, to Washington Headquarters Services, Directorate for Information Operations and Reports, 1215 Jefferson Davis Highway, Suite 1204, Arlington, VA 22202-4302, and to the Office of Management and Budget, Paperwork Reduction Project (0704-0188), Washington, DC 20503.

1. AGENCY USE ONLY (*Leave blank*)	2. REPORT DATE	3. REPORT TYPE AND DATES COVERED
	October 1995	Contractor Report

4. TITLE AND SUBTITLE
Simulation of Crossflow Instability on a Supersonic Highly Swept Wing

5. FUNDING NUMBERS
C NAS1-19656, Task 18

WU 505-59-50-02

6. AUTHOR(S)
C. David Pruett

7. PERFORMING ORGANIZATION NAME(S) AND ADDRESS(ES)
The College of William and Mary
Department of Applied Science
Williamsburg, VA 23185

8. PERFORMING ORGANIZATION REPORT NUMBER

9. SPONSORING / MONITORING AGENCY NAME(S) AND ADDRESS(ES)
National Aeronautics and Space Administration
Langley Research Center
Hampton, VA 23681-0001

10. SPONSORING / MONITORING AGENCY REPORT NUMBER
NASA CR-198267

11. SUPPLEMENTARY NOTES
Langley Technical Monitor: C. L. Streett
Final Report - Task 18

12a. DISTRIBUTION / AVAILABILITY STATEMENT
Unclassified - Unlimited

Subject Category 02

12b. DISTRIBUTION CODE

13. ABSTRACT (*Maximum 200 words*)

A direct numerical simulation (DNS) algorithm has been developed and validated for use in the investigation of crossflow instability on supersonic swept wings, an application of potential relevance to the design of the High-Speed Civil Transport (HSCT). The algorithm is applied to the investigation of stationary crossflow instability on an infinitely long 77-degree swept wing in Mach 3.5 flow. The results of the DNS are compared with the predictions of linear parabolized stability equation (PSE) methodology. In general, the DNS and PSE results agree closely in terms of modal growth rate, structure, and orientation angle. Although further validation is needed for large-amplitude (nonlinear) disturbances, the close agreement between independently derived methods offers preliminary validation of both DNS and PSE approaches.

14. SUBJECT TERMS
Compressible Flow
Crossflow Instability
High-Speed Civil Transport (HSCT)
Direct Numerical Simulation (DNS)
Parabolized Stability Equation (PSE) Methodology

15. NUMBER OF PAGES
38

16. PRICE CODE
A03

17. SECURITY CLASSIFICATION OF REPORT	18. SECURITY CLASSIFICATION OF THIS PAGE	19. SECURITY CLASSIFICATION OF ABSTRACT	20. LIMITATION OF ABSTRACT
Unclassified	Unclassified	Unclassified	

NASA Technical Library
3 1176 01423 8258